The pH dependence of the isotopic composition of boron adsorbed on amorphous silica

Giuseppe D. Saldi, Pascale Louvat, Jacques Schott, Jérôme Gaillardet

The pH dependence of the isotopic composition of boron adsorbed on amorphous silica

Giuseppe D. Saldi[1], Pascale Louvat[2], Jacques Schott[1] and Jérôme Gaillardet[2]

[1]*GET-CNRS-IRD, Université Paul Sabatier, 14 ave. Edouard Belin, 31400 Toulouse, France*
[2]*Institut de Physique du Globe de Paris, 1 rue Jussieu, 75238 Paris cedex 05, France*

Keywords: boron adsorption; boron isotope fractionation; amorphous silica; triple-layer model; B pH-proxy.

ABSTRACT

The use of the boron content and isotopic composition of secondary silicate minerals and siliceous organisms to trace weathering reactions and past ocean pH requires characterizing the fundamental reactions that govern the incorporation and subsequent isotope fractionation of this element in these materials. Toward this goal we have investigated boron adsorption on the surface of amorphous silica ($SiO_2 \cdot 0.32H_2O$) and quantified its isotopic fractionation. Boron adsorption envelopes and corresponding isotope fractionation factors were measured in dilute aqueous solutions (0.01 M) of NaCl and $CaCl_2$. B maximum adsorbed fraction was found to be about 2 times higher in $CaCl_2$ solutions than in NaCl. The modelling of chemical and isotopic data in NaCl solutions allowed to identify the formation of two main B surface species at the $SiO_{2(am)}$/water interface: a neutral trigonal (B3) inner-sphere complex, $>SiOB(OH)_2^0$, characterized by a fractionation factor of ~ -16 ‰ relative to aqueous boric acid, and a negatively charged tetrahedral (B4) inner-sphere complex, $>SiOB(OH)_3^-$, with fractionation factors of -5 ‰ with respect to aqueous borate. In $CaCl_2$ solutions the data modelling indicates the presence of B4 inner-sphere complexes with a fractionation factor of -6.5 ‰ relative to aqueous borate, but excludes the presence of trigonal surface species and suggests instead the formation of a $Ca\text{-}B(OH)_4^-$ complex that could partly account for the observed increase of boron adsorption in these solutions. These observations indicate that changes in the surface charge density and interfacial water structure due to different background electrolytes can induce changes in concentration and both chemical and isotopic composition of B adsorbed on silica surfaces.

Although this study suggests that the B adsorption reaction on $SiO_{2(am)}$ plays a minor role in the B incorporation and isotopic signature of clay minerals and siliceous cements forming during weathering reactions, the acquired data should allow for an improved knowledge of the biomineralization reactions. The observed B isotopic fractionations between adsorbed and aqueous B species should help determining the relative contribution of various processes, such as cellular transport, biological mediation and silicification reactions, on the amount of B incorporated in siliceous microorganisms and its isotopic signatures. In addition, the presence in NaCl solutions of both trigonal and tetrahedral boron complexes at the silica surface could explain the observed weak pH dependence of the boron isotopic composition of marine diatoms.

1. Introduction

In soils and weathering environments boron is mostly present in adsorbed form at the surface of clay minerals, metal oxides, calcium carbonate and organic matter (Goldberg, 1997), which control the concentrations of this element in aqueous solutions and its availability as micronutrient for plants (Keren et al., 1985; Goldberg, 2005; Cividini et al., 2010). Given the large chemical and isotopic fractionation values associated with boron adsorption reactions and incorporation in secondary phases (Schwarcz et al., 1969; Palmer et al., 1987; Spivack et al., 1987; Williams et al., 2001; Lemarchand et al., 2007), as well as vegetation cycling and evaporation-condensation processes, boron isotopes have been profitably used to trace chemical weathering reactions and to quantify the fluxes of matter between different compartments within the Critical Zone (Rose et al., 2000; Lemarchand and Gaillardet, 2006; Cividini et al., 2010; Lemarchand et al., 2012; Gaillardet and Lemarchand, 2018; Noireaux et al., 2021; Chetelat et al., 2021).

The study of boron sorption reactions on various soils and mineral surfaces has been extensive (e.g., Goldberg and Glaubig, 1986; Palmer et al., 1987; Goldberg et al., 1993; de Bussetti et al., 1995; Peak et al., 2003; Santos et al., 2020, and references therein), However, the mechanisms controlling the boron isotopic fractionation and composition of the complexes formed by adsorption at the surface of minerals have been the object of a limited number of studies, which examined the interaction of B with humic acid (Lemarchand et al., 2005) Fe- and Mn-oxides (Lemarchand et al., 2007), and calcite (Saldi et al., 2018). These studies showed how the reported B isotopic fractionation factors, with values ranging between –40 ‰ and +23 ‰, depend on both boron aqueous speciation and the pH-dependent distribution of differently fractionated trigonal and/or tetrahedral surface species.

The interactions of dissolved boron with silicate mineral surfaces, particularly clay minerals and various mineral coatings, strongly fractionate boron isotopes and control the chemical and isotopic composition of surface waters and groundwaters (e.g., Lemarchand and Gaillardet, 2006; Louvat et al., 2011; Gaillardet and Lemarchand, 2018; Noireaux et al., 2021). Therefore, the investigation of the specific mechanisms of B adsorption on these surfaces, which is generally the first step of boron incorporation in these solids, and associated isotopic fractionation, is much needed to extend the use of B isotopes and improve the estimates of B mass transfer during weathering reactions.

In the present contribution we examine the isotopic fractionation of boron during adsorption on amorphous silica ($SiO_2 \cdot 0.32H_2O$) as a function of aqueous solution pH. Although amorphous silica ($SiO_{2(am)}$) content is generally limited in soils, where it is primarily of phytogenic origin (cf. Farmer et al., 2005; Saccone et al., 2007), this phase is often observed as thin alteration layers on primary silicates along weathering profiles (Banfield and Eggleton, 1990; Hochella and Banfield, 1995; Zhu et al., 2006; Schindler et al., 2009; Hellmann et al., 2012; Schott et al., 2012) or adsorbed at the surface of Fe- and Al-oxides and hydroxides (Iler, 1979; Dietzel, 2002; Schindler and Hochella, 2015) and can constitute the primitive coatings from which clay minerals subsequently form (Charlet and Manceau, 1994; Nugent et al., 1998; Schindler and Singer, 2017). Locally, $SiO_{2(am)}$ can also precipitate from supersaturated solutions at the base of the soil profile (e.g., Alexandre et al, 1997) and is found to form silicretes within the regolith-groundwater system, where it can impregnate the clay-rich matrix and constitute the main cementing phase (e.g., Drees et al., 1989; Lee and Gilkes, 2005; Basile-Doelsch et al., 2005; Thiry et al., 2006).

The quantification of B adsorption on $SiO_{2(am)}$ and the determination of the isotopic fractionation accompanying the formation of the B surface species involved in this reaction is therefore fundamental to understand the mechanisms whereby boron fractionates between aqueous solution and weathering products. Considering the relative abundance and high specific surface area of SiO_2-rich surface layers it is possible that the isotopic signature of clay minerals and other secondary phases be partly inherited from the boron adsorbed or coprecipitated with pre-existing $SiO_{2(am)}$ coatings.

The determination of the abundance and isotopic composition of the boron adsorbed at the $SiO_{2(am)}$ surface is also of great interest to assess the implication of the adsorption reaction in the incorporation of this element by siliceous micro-organisms (diatoms, sponges and radiolarians). Although the overall process of silicification is very complex and mediated by different biological factors (Vrieling et al., 1999; Martin-Jézéquel et al., 2000; Schröder et al., 2004), this study should allow for a better characterization of the reaction pathways that control boron content and isotopic signatures in biogenic silica and could ultimately help to extend the application of the B isotope pH-proxy to siliceous organisms (cf. Eggins et al., 2004; de Leon et al., 2009; Donald et al., 2020).

To the best of our knowledge the adsorption of boron on silica surfaces was investigated in two distinct studies without the determination of the corresponding B isotope fractionations. Tanifuji et al. (2009) measured the adsorption of B on silica gel as a function

of pH and B aqueous concentration using different pH-adjusting metal hydroxides and reported an increased adsorption of B in alkaline-earth solutions compared to alkali metals aqueous solutions. These authors did not characterize the identity of the surface species formed by the adsorbed boron. In another study Kim and Kirkpatrick (2006) used NMR spectroscopy to characterize the B species adsorbed on the surface of silica gel at different pH's. It was suggested that the adsorption of both trigonal (B3) and tetrahedral (B4) occurs principally as outer-sphere complexes, with the relative abundance of B4 being greater than in solution. Starting from these observations we conducted an experimental study aimed at measuring B adsorption on $SiO_{2(am)}$ in aqueous solutions of NaCl and $CaCl_2$ for the determination of the surface complexes formed by B with amorphous silica surface functional groups and the corresponding isotope fractionation factors. Our results allow to quantify the possible contribution of B adsorption reaction on amorphous silica to the processes of B incorporation into weathering products and provide useful information for a better understanding of the mechanisms that control the B isotopic composition of marine siliceous organisms.

2. Experimental Methods

2.1 Materials and experimental protocol

Reagent grade amorphous silica from Alfa Aesar (silicic acid hydrate, $SiO_2 \cdot 0.32H_2O$) was used in this study. Three different batches of the same powder were repeatedly washed and allowed to settle for half an hour between each washing cycle at the bottom of large glass beakers. Each time the supernatant containing ultrafine particles was removed and the remaining solid was dried in an oven at 60 °C for 6 days. The final silica powder consisted of aggregates of nanoparticles having size of 20-40 nm, as shown by transmission electron microscope (TEM, Jeol JEM-ARM 200F) in Fig. 1. The specific surface area (SSA) of the prepared powders was measured by 11-point BET method using N_2 as adsorbate, which provided SSA values of 159-188 m^2/g with an uncertainty within ± 5%.

A first series of adsorption experiments was conducted using two aqueous solutions of NaCl at a concentration of 0.0065 M and containing either 0.0035 mol/kg of $NaHCO_3$ or 0.0035 mol/kg of Na_2CO_3. A volume of 500 ml of these two solutions was left in contact with 2 g of the same silica powder and mixed in a shaking bath for three weeks, then filtered with Millipore PTFE filters at 0.20 µm and stored in PET bottles to be used for the experiments. A

second series of experiments was conducted using a solution of $CaCl_2$ 0.01 M, again pre-equilibrated with $SiO_{2(am)}$ according to the same protocol, to study the effect of Ca on the amount and isotopic composition of adsorbed boron.

All the experiments were carried out in 50 ml polypropylene (PP) centrifuge tubes at 21 ± 1 °C using 5.5-6 g of silica powder and 25 ml of aqueous solution. The suspensions were continually mixed for at least 24 hours with a tube rotator and the pH adjusted to the desired values by adding small amounts of 0.1 or 1 M NaOH solutions before B addition. Boron stock solutions at 125 ppm were prepared from analytical grade H_3BO_3 in 0.01 M NaCl and $CaCl_2$ solutions. 1 ml of B stock solution was added to each suspension to obtain an initial concentration of ~5 ppm and replicate the current concentration levels measured in seawater. After B addition, the suspensions were mixed for a period of 5-6 hours. Although this time interval seemed to be sufficient to attain constant levels of B adsorbed onto the silica powder, a time series in which B was left in contact with the suspension at pH 9 for longer time periods, up to 48 hrs, was conducted to check for possible variations of B adsorbed fraction and isotopic composition. Once the agitation was stopped, the tubes were centrifuged for 15 minutes at a speed of 8500 rpm while keeping a constant temperature of 21 °C within the centrifuge basket. The aqueous solution was collected from each tube with a sterile plastic syringe and filtered using 0.20 µm PTEF filters for chemical and B isotope analyses. Note that the use of 0.20 µm filters was sufficient to prevent significant amount of $SiO_{2(am)}$ particles from being collected within the aqueous solution. Several solution samples were also filtered at 20 nm and measured B and Si concentrations were observed to correspond within uncertainties to those determined in the samples filtered only at 0.20 µm. A separate aliquot of solution was collected immediately after centrifugation without filtering for the pH determination. A Metrohm pH microelectrode calibrated against NIST certified buffers was used for this purpose.

2.2 Chemical and isotopic analyses

B, Si and Ca aqueous concentrations were measured by inductively coupled plasma optical emission spectroscopy (ICP-OES) at GET laboratory in Toulouse using a Horiba Ultima 2 spectrometer equipped with a nebulizer and a cyclonic spray chamber made of Teflon and Peek parts to prevent boron contamination and memory effects that would result from the contact of fluid samples with glass components (cf. Sah and Brown, 1997). The uncertainty of the fluid analyses was generally lower than 2% with detection limits of 7, 10 and 11 ppb for B, Ca and Si, respectively.

Prior to boron isotope analyses, B was extracted from the sample solutions using ion exchange chromatography on gravimetric columns loaded with 50 µL of the anionic resin Amberlite IRA 743, specific to boron. A small aliquot of the sample solution (3 to 150 µL, calculated for 350 ng of B) was diluted to 0.5 mL with high purity water (Milli-Q from Millipore-ThermoScientific) and basified to pH 8-9 with micro-droplets of distilled 4M NH_4OH, when needed. The samples were introduced to the chromatography columns pre-conditioned with Milli-Q water at pH 9. After rinsing the resin with Milli-Q water at pH 9, 2.6 M $NaNO_3$, and Milli-Q water at pH 9 again, the boron was recovered with 50 µL of 0.5 N HNO_3 and 600 µL of 0.1 N HNO_3. The sample was further diluted with 1.05 mL of Milli-Q water to reach a final B concentration of 200 ppb in 0.05 N HNO_3 for isotopic analyses. Total procedure blanks (TPBs) and seawater were also processed for each batch of ten samples. TPBs and boron concentrations of the sample after boron extraction were measured at the MC-ICP-MS Neptune (ThermoScientific) at IPGP by calibrating ^{11}B intensity on B standard solutions, at 1 ppb for the TPB and 200 ppb for the samples. For this series of samples the TPBs were of 150 ± 40 pg (2SD, n=5) of B and were considered negligible compared to the 350 ng of B in the samples. B concentrations in the samples were all very close to 200 ppb, attesting for a complete extraction of B from the samples.

B isotope ratios were measured on the MC-ICP-MS Neptune (ThermoScientific) at IPGP with a micro sample introduction system using a direct injection nebulizer directly plugged in the torch (Louvat et al., 2019). Samples were measured in triplicate and the instrumental mass bias was corrected through standard-sample-standard bracketing (SSB) with the standard reference material NIST SRM 951 (Catanzaro et al., 1970). $\delta^{11}B$ values were directly calculated from the measured $^{11}B/^{10}B$ ratios. Sample and bracketing standard concentrations were closely matched to within 5%. Stability and accuracy of the boron isotope ratio measurements were assessed by regularly measuring the standard reference materials BAM AE120, AE121 and AE 122 (Vogl and Rosner, 2011). Long-term average of $\delta^{11}B$ measurements of these reference materials at IPGP are -20.31 ± 0.19 ‰ (n=16), 19.58 ± 0.18 ‰ (n=59) and 39.35 ± 0.21 ‰ (n=22) for AE120, AE121 and AE122, respectively (Louvat et al., 2019, errors in 2SD), and agree with the gravimetric reference values (-20.2 ± 0.6 ‰, 19.9 ± 0.6 ‰ and 39.9 ± 0.6 ‰, respectively; Vogl and Rosner, 2011), and even better with the values measured by Donald et al. (2020). The $\delta^{11}B$ values for the seawater NASS aliquots that were processed together with the samples for B extraction were reproducibly measured at 39.65 ± 0.25 (2SD, n=5) in perfect agreement with the seawater $\delta^{11}B$ value proposed by

Foster et al. (2010). The average $\delta^{11}B$ values and errors (expressed as 2 standard deviation) given for each sample in Table 5 are calculated from the five $\delta^{11}B$ values determined by the triplicate SSB analysis (Louvat et al., 2014).

2.3 Boron sorption modelling

Boron sorption at the amorphous silica surface was modelled using the triple-layer model (TLM) originally developed by Yates et al. (1974) and Davis and Leckie (1978) to describe the adsorption of metal ions at the oxide/water interface. A large number of studies adopted and modified the TLM to interpret the adsorption of ions on different solids and in particular on silica surfaces (e.g., Schindler and Stumm, 1987; Kosmulski, 1996; Sahai and Sverjensky, 1997a; Icenhower and Dove, 2000; Berka and Bányai, 2001; Sverjensky, 2006; Carroll et al., 2008).

According to the TLM, the adsorption of ions at the aqueous solution-solid interface takes place at three idealized mean planes (0-, β- and d-plane), which define the electrical double-layer (EDL) and the diffuse layer where aqueous species and electrolyte ions adsorb to form inner-sphere and outer-sphere complexes and neutralize the charge developed at the solid surface. Within this formalism the sorption of protons and hydroxyl groups is located at the 0-plane, whereas the adsorption of the other ions occurs between the 0-plane and the β-plane and occasionally at the d-plane (cf. Sverjensky, 2006). The surface charges (σ_i) and potentials (ψ_i) developed at these planes are related by the integral capacitance C_1 and C_2 [F/m^2] of the intervening charged layers according to the following equations:

$$\sigma_0 = C_1(\psi_0 - \psi_\beta) \quad (1)$$

$$\sigma_\beta = C_2(\psi_\beta - \psi_d) , \quad (2)$$

where C_1 and C_2 are assumed to be constant. The reactions and EDL parameters that define the TLM used in the present study to describe the $SiO_{2(am)}$ surface speciation are summarized in Table 1. For the silanol groups (>SiOH^0) that constitute the $SiO_{2(am)}$ reactive sites, the reactions of protonation and deprotonation can be expressed as follows:

$$>SiOH^0 + H^+ = >SiOH_2^+ \quad (3)$$

$$>SiOH^0 = >SiO^- + H^+ . \quad (4)$$

for which the corresponding equilibrium constants are defined by:

$$K_{>SiOH_2^+} = \frac{\{>SiOH)_2^+\}}{\{>SiOH^0\} \cdot a_{H^+}} \, exp\left(-\frac{F\psi_0}{RT}\right) , \quad (5)$$

$$K_{>SiO^-} = \frac{\{>SiO^-\} \cdot a_{H^+}}{\{SiOH^0\}} \, exp\left(-\frac{F\psi_0}{RT}\right), \quad (6)$$

where F is the Faraday constant, R is the gas constant, the curly brackets identify the concentration of the indicated surface species and a_{H^+} designates the activity of H^+. Note that the values of the intrinsic constants of formation of the surface species involved in the model (Table 1) were taken from the literature, except for the value of the constant of deprotonation of the silanol groups ($K_{>SiO^-}$) and the constant of formation of Ca surface complexes, which were obtained by fitting of our experimental data. The use of a fitted value for this Log $K_{>SiO^-}$ was necessary because of the variability of this constant, as indicated by the wide range of values provided in the literature (see § 4.1.1), whereas the high measured fractions of adsorbed Ca were not consistent with the intrinsic stability constants available in the literature and required the determination of new constants that could account for the measured Ca concentrations (see § 3.2.2).

In modelling the B adsorption data both trigonal and tetrahedral B surface species were allowed to form at the $SiO_{2(am)}$-interface, in accord with the adsorption scheme adopted for Fe and Mn- oxides (Lemarchand et al., 2007). In terms of the basic thermodynamic species the formation of these surface complexes can be therefore described by the following reactions:

$$>SiOH^0 + B(OH)_3^0 = >SiOB(OH)_2^0 + H_2O \quad (7)$$

$$>SiOH^0 + B(OH)_3^0 = >SiOH_2^+\text{-}BO(OH)_2^- \quad (8)$$

$$>SiOH^0 + B(OH)_3^0 = >SiOB(OH)_3^- + H^+ \quad (9)$$

$$>SiOH^0 + B(OH)_3^0 + H_2O = >SiOH_2^+\text{-}OB(OH)_3^{2-} + H^+ \quad (10)$$

where $>SiOB(OH)_2^0$ and $>SiOH_2^+$-$BO(OH)_2^-$represent respectively the trigonal (B3) inner-sphere and outer-sphere surface complexes and $>SiOB(OH)_3^-$ and $>SiOH_2^+$-$OB(OH)_3^{2-}$ are the tetrahedral (B4) inner-sphere and outer-sphere complexes. The existence of trigonal and tetrahedral B surface species forming both inner- and outer-sphere complexes was suggested by ^{11}B MAS NMR analyses conducted by Kim and Kirkpatrick (2006) on B adsorbed onto silica gel.

The intrinsic constants of formation of the four B surface species defined above are expressed by the following equations:

263 $$K_{B3-is} = \frac{\{>SiOB(OH)_2^0\}}{\{SiOH^0\}\cdot a_{B(OH)_3^0}}\ exp\left(-\frac{F\psi_0}{RT}\right) \quad (11)$$

264 $$K_{B3-os} = \frac{\{>SiOH_2^+ - B(OH)_2^-\}}{\{SiOH^0\}\cdot a_{B(OH)_3^0}}\ exp\left(-\frac{F(\psi_0-\psi_\beta)}{RT}\right) \quad (12)$$

265 $$K_{B4-is} = \frac{\{>SiOB(OH)_3^-\}\cdot a_{H^+}}{\{SiOH^0\}\cdot a_{B(OH)_3^0}}\ exp\left(-\frac{F\psi_0}{RT}\right) \quad (13)$$

266 $$K_{B4-os} = \frac{\{>SiOH_2^+ - OB(OH)_3^{2-}\}\cdot a_{H^+}}{\{SiOH^0\}\cdot a_{B(OH)_3^0}}\ exp\left(-\frac{F(\psi_0-2\psi_\beta)}{RT}\right), \quad (14)$$

267 where the curly brackets designate the concentration of the indicated surface species and a_i
268 correspond to the activity of the subscripted aqueous species. The determination of the
269 intrinsic stability constants of the B surface species was accomplished by iterative modelling
270 of the adsorption data with Visual Minteq v.3.1 (Gustafsson, 2012) and its integrated PEST
271 optimization procedure (Doherty, 2010). The code provided at the same time the distribution
272 of all adsorbed and dissolved aqueous species that describe our system. Before starting the
273 modelling calculations the constant of formation of the aqueous complex $NaHSiO_3^0$ (log K = -
274 8.30; Johnson et al., 1992) was added to the thermodynamic database, as a significant fraction
275 aqueous silica is predicted to be present as this complex at basic pH. The inner and outer
276 capacitances, C_1 and C_2, were used as fitting parameters and fixed respectively to values of
277 2.2 and 0.05 F/m^2, which provide the best fit of all data and are within the interval of values
278 typical of the silica-water interface (cf. Kosmulsky et al., 1999; Sverjensky, 2001; Carroll et
279 al., 2008). The total surface site density of the silanol groups was assumed to be equal to 4.6
280 nm^{-2}, in agreement with several other studies that investigated and modelled sorption
281 reactions at the amorphous silica/water interface (e.g., Sahai and Sverjensky 1997a;
282 Zhuvralev, 2000; Sverjensky, 2006; Carroll et al., 2008).

283 **2.4 Isotopic calculations**

284 The isotopic composition of the boron adsorbed at the amorphous silica surface ($\delta^{11}B_{ads}$)
285 was deduced from the isotopic ratio measured in the aqueous samples ($\delta^{11}B_{sol}$) according to
286 the following mass conservation equation:

287 $$\delta^{11}B_{ads} = \frac{\delta^{11}B_0 - \delta^{11}B_{sol}\cdot(1-X)}{X}\ , \quad (15)$$

where $\delta^{11}B_0$ represents the isotopic composition of the initial boron stock solution and X corresponds to the measured fraction of adsorbed B derived from aqueous solution analyses according to:

$$X = \frac{[B]_0 - [B]_{sol}}{[B]_0} \quad , \tag{16}$$

where $[B]_0$ corresponds the concentration of aqueous boron at the beginning of each experiment and $[B]_{sol}$ is the aqueous boron concentration measured at the end of the experiment.

The boron isotopic fractionation factor between the $SiO_{2(am)}$ surface and the aqueous solution, $\alpha_{ads\text{-}sol} = \frac{(^{11}B_{ads})/(^{10}B_{ads})}{(^{11}B_{sol})/(^{10}B_{sol})}$, was calculated for each data point by the following expression (cf. Johnson et al., 2004):

$$\alpha_{ads\text{-}sol} = \exp\left(\frac{\delta^{11}B_{ads} - \delta^{11}B_{sol}}{1000}\right) = \exp\left(\frac{\Delta^{11}B_{ads-sol}}{1000}\right). \tag{17}$$

Assuming the formation of the four surface species defined by reactions (7-10), a boron isotope fractionation factor between each surface complex and aqueous boric acid can be defined according to:

$$\alpha_{B3-is} = \frac{(^{11}B/^{10}B)_{>SiOB(OH)_2^0}}{(^{11}B/^{10}B)_{B(OH)_3^0}}, \tag{18a}$$

$$\alpha_{B3-os} = \frac{(^{11}B/^{10}B)_{>SiOH_2^+ - BO(OH)_2^-}}{(^{11}B/^{10}B)_{B(OH)_3^0}}, \tag{18b}$$

$$\alpha_{B4-is} = \frac{(^{11}B/^{10}B)_{>SiOB(OH)_3^-}}{(^{11}B/^{10}B)_{B(OH)_3^0}}, \tag{18c}$$

$$\alpha_{B4-os} = \frac{(^{11}B/^{10}B)_{>SiOH_2^+ - OB(OH)_3^{2-}}}{(^{11}B/^{10}B)_{B(OH)_3^0}} \tag{18d}$$

The overall B isotopic fractionation factor between the amorphous silica surface and the aqueous solution can be expressed as a function of the fraction of the different B surface complexes and their fractionation factors relative to boric acid according to (cf. Lemarchand et al., 2007; Saldi et al., 2018):

$$\alpha_{ads-sol} = \frac{\sum[\{>SiO-B_i\}\cdot\alpha_{Bj-z}]}{[B(OH)_3^0]+[B(IV)]_t\cdot\alpha_{4-3}} \cdot \frac{[B(OH)_3^0]+[B(IV)]_t}{\sum\{>SiO-B_i\}}, \tag{19}$$

where $\{> SiO - B_i\}$ stands for the concentration of the i*th* surface complex formed by B with the silica functional groups (reactions 7-10); α_{Bj-z} represents the B fractionation factor between the i*th* surface complex and boric acid, with the subscript *j* defining the adsorbed B species coordination (3 or 4) and *z* identifying either an inner-sphere (*is*) or an outer-sphere (*os*) complex (Eq. 18a-d); α_{4-3} is the fractionation factor between the borate ion and boric acid, and $[B(IV)]_t$ is the concentration sum of all dissolved tetrahedral B species present in the aqueous solution: $B(OH)_4^-$, $NaB(OH)_4^0$, and $CaB(OH)_4^+$.

Modeled $\alpha_{ads\text{-}sol}$ values were obtained from the experimentally measured α values and the calculated distribution of B aqueous and surface species by a least square fitting of Eq. (19), using α_{B3-is}, α_{B3-os}, $\alpha_{B4-is}$and α_{B4-os} as fitting parameters for a fixed value of α_{4-3} (see below).

3. Results

3.1 B adsorption envelopes

The results of B adsorption on amorphous silica as a function of pH in 0.01 M NaCl and $CaCl_2$ aqueous solutions are reported on the plots of Fig. 2 and summarized in Table 2 and 3. The distributions of the B adsorption data as a function of pH are bell-shaped, with maximum adsorbed B amounts at pH ≈ 9. The percentage of adsorbed boron varies between 8 and 41 % in NaCl solutions with maximum values (B_{ads} = 7.5-9.7 µg/g) at 8.6< pH< 9.5, whereas it is 1.2 to 3 times higher in $CaCl_2$ solutions, varying between 12 and 65 %, with the highest adsorbed amounts (B_{ads} = 12.2-15.3 µg/g) at 8.2< pH< 9.1. This observation is consistent with the reported increase of B adsorbed on silica gel in alkaline earth metal-bearing solutions relative to Na- and K-bearing solutions (Tanifuji et al., 2009). The results of additional three experiments in 0.01 M NaCl at pH=9, where added boron was left in contact with the $SiO_{2(am)}$ suspension for 5.5, 24 and 48 hours, show that the extent of adsorption increased by 24 % after 24 h and 32 % after 48 h. The apparent increase of adsorption with time is believed to be due to deagglomeration of the SiO_2 powder and the subsequent increase of the interfacial surface area. The isotopic analysis of these samples show, however, that boron fractionation factor between amorphous silica and the fluid was not affected by the increase of adsorption extent within analytical uncertainties, as shown on the plot of Fig. 3b.

It must be noted that the surface area-normalized adsorption values reported in the Tables and Fig. 2 are 4-5 times lower than those measured on calcite (Goldberg and Forster, 1991;

Saldi et al., 2018) but also lower than the amounts adsorbed on various soil samples, clay minerals and Fe-oxides (cf. Goldberg and Glaubig, 1986; Goldberg et al., 1993; Lemarchand et al., 2007; Gaillardet and Lemarchand, 2018; Santos et al., 2020), indicating the relatively low affinity of B for $SiO_{2(am)}$ surfaces.

3.2 B isotopic data

The results of boron isotope analyses for the sorption experiments conducted in NaCl and $CaCl_2$ aqueous solutions are reported in Table 4. For each run are listed the B fraction adsorbed at the silica surface, the $\delta^{11}B_{sol}$ values measured at the end of the run along with the calculated values of $\delta^{11}B_{ads}$ and the corresponding B fractionation factors ($\Delta^{11}B_{ads\text{-}sol}$ and $\alpha_{ads\text{-}sol}$). The isotope compositions of aqueous B are plotted as a function of pH in Fig. 3a. It can be seen that the measured isotopic composition of the $CaCl_2$ solutions is 5-10 ‰ heavier than that of the NaCl solutions for the same pH conditions. Note that the measured isotopic composition of the two stock solutions prepared with NaCl ($\delta^{11}B_0$ = -0.05 ±0.06 ‰) and $CaCl_2$ ($\delta^{11}B_0$ = -0.15 ±0.06 ‰) is the same within errors. The different behavior of B isotopes in the two electrolyte solutions is illustrated by the respective variation of the isotope fractionation factor between the $SiO_{2(am)}$ surface and the fluid ($\alpha_{ads\text{-}sol}$) as a function of pH (Fig. 3b). The data obtained from the experiments conducted in NaCl solutions are distributed along a v-shaped pattern, with $\alpha_{ads\text{-}sol}$ decreasing with increasing pH from 0.985 ($\Delta^{11}B_{ads\text{-}sol}$ = -15.6 ‰) to 0.970 ($\Delta^{11}B_{ads\text{-}sol}$ = - 30 ‰) at 6.5 < pH < 8.3 and then systematically increasing with increasing pH up to a value of 0.998 ($\Delta^{11}B_{ads\text{-}sol}$ = -1.6 ‰) at pH = 10.55. Therefore, adsorbed boron displays two opposite trends with respect to pH, with highest enrichment in ^{10}B at pH of 8.1-8.4 and compositions that are progressively enriched in ^{11}B as the fluid pH becomes either more acidic or more alkaline. Such a bidirectional dependence on pH is not observed for the data acquired in $CaCl_2$ solutions, where the fractionation factors between $SiO_{2(am)}$ and aqueous solution appear to follow the variation of the isotopic composition of $B(OH)_4^-$ (dashed line on the plot), although with compositions of adsorbed B that are 4 to 8 ‰ lighter than those of the dissolved anion for the considered fractionation factor between boric acid and borate ion ($\alpha_{3\text{-}4}$ = 1.027; Klochko et al., 2006; see next section). Similar isotope fractionation values can be observed in NaCl solutions at pH > 8.

3.3 B adsorption modelling

3.3.1 B adsorption models in NaCl solutions

In modelling the B adsorption data within the single site TLM we considered i) the adsorption of Na^+ at the β-plane (reaction 3 in Table 1) using the intrinsic constant value from

Komulski (1997), which accounts for the Na sorption observed in our experiments, and ii) the formation of B3 and B4 surface species, present both as inner-sphere and outer-sphere complexes, as described by reactions (7-10). Our results allow to exclude the presence of outer-sphere trigonal B complexes [$>SiOH_2^+$-$BO(OH)_2^-$] but suggest the formation of the inner-sphere trigonal species, $>SiOB(OH)_2^0$, along with inner- and outer-sphere tetrahedral surface species, $>SiOB(OH)_3^-$ and $>SiOH_2^+$-$B(OH)_3^-$. The modelling of the data involved the fitting of the silanol deprotonation constant, $K_{>SiO^-}$, which was optimized to reach the best agreement between the measured adsorption envelope and the models considered. It has to be noted that five data points were excluded from the fitting procedure (empty symbols in Fig. 2a) as they represent either independent replicate values that differ significantly from other data obtained at the same pH and from the main distribution, or values that compromised the numerical convergence of the model and were possibly affected by some experimental artifact.

The values of the intrinsic stability constants determined for the B surface complexes are reported in Table 5 and were obtained for Log $K_{>SiO^-}$ = -11.0. The good agreement between the model predictions and the experimental data (R=0.99) can be viewed in the plot of Fig. 2a (dashed blue line). The derived distribution as a function of pH of the B species involved in the adsorption process is illustrated in Fig. 4a. The trigonal surface species is dominant in the near-neutral pH region, up to pH 7.5, whereas the inner-sphere B4 surface complex is the most abundant species at more alkaline pH's, with a maximum concentration at pH ~ 9.2. The relative concentration of the outer-sphere B4 complex increases with pH reaching values of 35-38 % between pH 10.5 and 12.0. The formation of B4 outer-sphere complexes is consistent with the interpretation of NMR measurements by Kim and Kirkpatrick (2006) and may also be expected owing to the low dielectric constant of amorphous silica relative to other solids (cf. Sverjensky, 2006)[1]. However, the validity of this model must be ultimately confirmed by the consistency of the corresponding isotope fractionation factors calculated for the modelled B surface species (§ 3.4).

An adsorption model involving the formation of only inner-sphere surface species was also tested and provided log K_{int} values equal to -0.56 ± 0.23 and -7.64 ± 0.06 for, respectively, the trigonal [$>SiOB(OH)_2^0$] and tetrahedral [$>SiOB(OH)_3^-$] surface complexes. It can be seen on the plot of Fig. 2a (continuous green line) that the agreement of this model with the data

[1] The Born solvation contribution to the Gibbs free of a cation adsorption depends primarily on the inverse of the dielectric constant of the solid (Sahai and Sverjensky, 1997b).

(R=0.98) is as good as the one achieved by the three-species model and no real difference exists between the two. Note that according to the two-species model the concentration of the trigonal B complex is ~ 25% lower than predicted by the three-species model that includes the formation of an outer-sphere tetrahedral complex (Fig. 4b).

3.3.2 B adsorption model in $CaCl_2$ solutions

The accurate determination of B intrinsic stability constants in $CaCl_2$ solutions required a new estimate of the constants of Ca adsorption at the silica surface such that they could describe the drop of Ca aqueous concentration observed in our experiments (Table 3). Previous studies described the adsorption of Ca on amorphous SiO_2 with the formation, as in the case of Na sorption, of mononuclear complexes at the β-plane according to:

$$>SiOH^0 + Ca^{2+} = >SiO^-\text{-}Ca^{2+} + H^+, \quad (20)$$

providing log K_{int} values ranging from -6.9 for silica gel at 20 °C (Berka and Bányai, 2001) to -5.2 for amorphous silica between 15 and 35°C (Kosmulski, 1994). The adoption of this reaction with the reported equilibrium constant values greatly underestimate the extent of Ca adsorption observed in our experiments and prevents a good description of B adsorption data.

In modelling Ca adsorption on SiO_2, Sverjenski (2006) considered the alternate formation of two, both protonated and non-protonated, tetranuclear species but also showed that the presence of Ca species at the *d*-plane could account for a significant fraction of adsorbed Ca, particularly at low ionic strengths (see also Pivovarov, 2010). Subsequently, in addition to reaction (20) we also considered the following surface reaction describing the formation Ca species at the *d*-plane:

$$>SiOH^0 + Ca^{2+} = >SiO^-\cdots Ca^{2+} + H^+ \quad (21)$$

The combination of reaction (20) and (21) allows a better description of the amount of Ca adsorbed as a function of pH than reaction (20) alone (Fig. 5), with log K_{int} values for reaction (20) and (21) of -3.8 ± 0.4 and -6.5 ±0.5, respectively.

Taking account of the intrinsic constants obtained for the formation of Ca surface complexes, the distribution of the B adsorption data as a function of pH can be described by the formation of an inner-sphere tetrahedral surface species [$>SiOB(OH)_3^-$] according to reaction (9) and a [$>SiO^-\text{-}CaB(OH)_4^+$] surface complex, which accounts for less than 23 % of total adsorbed boron and is described by the following reaction:

$$>SiO\text{-}Ca^{2+} + B(OH)_4^- = >SiO^-\text{-}CaB(OH)_4^+ \quad (22)$$

The values of the formation constants of these two surface complexes are reported in Table 5 and the resulting B adsorption model is illustrated in the plot of Fig. 2b, whereas the corresponding distribution of the two surface species as a function of pH is shown in Fig. 4c. Note that the introduction of an outer-sphere B-complex would lead to a poorly constrained value of $K_{\text{B4-os}}$ and a poor agreement between the model and the data. For the same reason the adsorption of boric acid was not considered.

3.4 Boron isotopic fractionation modelling

The B fractionation factors of tetrahedral and trigonal surface species relative to dissolved boric acid were determined from the overall experimental B fractionation factors via a least square fitting method using Eq. (19). The values of the fractionation factors relative to the identified adsorbed species – α_{B3-is}, $\alpha_{B4-is}$and α_{B4-os} – were incrementally varied to obtain the best fit curve that minimized the residual sum of squares between the model and the data. In modelling the experimental data, a choice on the value of the fractionation factor between borate ion and boric acid (α_{4-3}) has to be made. Different values of α_{3-4}, ranging from 1.025 to 1.031 were determined and adopted in previous studies (e.g., Liu and Tossel, 2005; Klochko et al., 2006; Noireaux et al., 2015; Nir et al., 2015; Kaczmarek et al., 2016; Saldi et al., 2018; Farmer et al., 2019). While there is no clear evidence about the sensitivity of α_{3-4} to ionic strength and aqueous solution composition, the fractionation factor determined by Klochko et al. (2006) for synthetic seawater (α_{3-4} = 1.0272; α_{4-3} = 0.9735) is one of the most used, particularly in the study of marine carbonates, but can be representative as well of more dilute solutions (cf. Liu and Tossel, 2005; Rustad et al., 2010; Nir et al., 2015). For sake of comparison with other works and our previous study on calcite (Saldi et al., 2018) this value of α_{3-4} was adopted in our analysis.

The results of the models for the data obtained in NaCl and $CaCl_2$ solutions are displayed on the plots of Fig. 6 and the corresponding values of the fractionation factors between each surface species and boric acid are listed in Table 5. For the NaCl solutions the calculated curve describing the variation with pH of the B overall fractionation factor was obtained for α_{B3-is}= 0.9849 (± 0.0030), α_{B4-is}= 0.9589 (± 0.0024) and α_{B4-os}= 0.9861 (± 0.0024) in the case of the model including both inner- and outer-sphere B4 complexes (Fig. 6a), whereas for the other model (Fig.6b) the calculated values of the two inner-sphere complexes were α_{B3-is}= 0.9841 (± 0.0025) and α_{B4-is}= 0.9685 (± 0.0020). It should be noted that the choice of a different value of α_{3-4} would have a limited impact on the modeled B isotope fractionation values of the adsorbed species. For α_{3-4} = 1.031, corresponding to the value

proposed by Klochko et al. (2006) for pure water, the fractionation factors of trigonal and tetrahedral B adsorbed species would be, respectively, 2‰ and 1.5 ‰ smaller than calculated for α_{3-4} = 1.027.

In the $CaCl_2$ solutions (Fig. 6c) the inner-sphere tetrahedral surface complex fully accounts for the measured B fractionation at pH≤ 8.2 with a fractionation factor relative to aqueous borate equal to -6.5 ‰ (α_{B4-is}= 0.9671 ± 0.0017). At pH > 8.2, in addition to the tetrahedral inner-sphere complex, the formation of the surface complex $>SiO^{-}$-$CaB(OH)_4^{+}$ accounts for more than 5% of the adsorbed B fraction and contributes to the overall fractionation with a value of its fractionation factor comprised between that of α_{B4-is} and α_{4-3}. Although the number of data points does not allow for a precise estimate of its fractionation factor, this complex should not be lighter than 1.5-2.0 ‰ relative to the borate ion in solution. The model of Fig. 6c was obtained assuming a fractionation of -1.1 ‰ with respect to aqueous $B(OH)_4^{-}$ (α_{Ca-B4}= 0.972).

The modelled values of the B fractionation factor in NaCl solutions indicate a substantial change of isotopic composition between the species adsorbed at the silica surface and the aqueous fluid. In the three-species model both inner-sphere trigonal and tetrahedral B surface complexes are more than 14 ‰ lighter than their dissolved counterparts, whereas the outer-sphere tetrahedral complex, $>SiOH_2$-$OB(OH)_3^{2-}$, is predicted to be heavier by almost 13‰ than $B(OH)_4^{-}$ in solution. For the two-species model, involving the formation of two inner-sphere surface complexes, the fractionation factors between adsorbed B3 and B4 species and their dissolved counterparts are equal to ~ -16 and -5 ‰, respectively. It must be noted that the isotopic composition of the adsorbed B4 complex is in this case similar to that obtained for $CaCl_2$ solutions. This model (Fig. 6b) provides a less accurate fit to the measured isotopic fractionation compared to the model involving both inner- and outer-sphere B4 species (Fig. 6a), particularly at 8 ≤ pH < 9 and at very alkaline pH, but does not present the strong contrast in fractionation between the inner-sphere and the outer-sphere tetrahedral species (~27 ‰ difference). These two species having the same coordination, such a difference in isotopic composition makes the model rather improbable.

The evident differences in the B surface complexation behavior and the accompanying isotopic fractionation between NaCl and $CaCl_2$ solutions point to the contrasting effect of dissolved alkaline and alkali-earth chlorides on the silica surface properties (see § 4.1.2).

4. Discussion

The adherence of the B isotope fractionation models presented above to the experimental data relies upon i) the accuracy of the interpretation of the adsorption data, i.e., the probability of formation of the postulated B surface species and ii) the relevance of the values assigned to the fractionation factors of these species. These two critical aspects of the data interpretation are discussed below.

4.1 The accuracy of boron adsorption models

4.1.1 Silanol groups deprotonation constant

To generate a model that could properly account for the measured values of B adsorption we had to use a self-consistent set of intrinsic constants that define the speciation at the $SiO_{2(am)}$/fluid interface. This involved the derivation of a value of the deprotonation constant of the silanol groups ($K_{>SiO^-}$) operating both in NaCl and $CaCl_2$ solutions, and a new value for the constant of Ca adsorption on the silica surface. Except for these two surface reactions, the other constants reported in Table 1 are consonant with most literature data and, with the exclusion of the Na surface complex, their variation does not significantly affect the results of the model. The use of a fitted value for the deprotonation constant of the silanol groups was made necessary by the lack of coherence between measured and modelled sorption envelopes when adopting the $K_{>SiO^-}$ values provided by different literature works, which range between $10^{-5.7}$ and $10^{-9.6}$ (cf. Bousse and Meindl, 1986; Persello, 2000; Icenhower and Dove, 2000; Carrol et al., 2002; Fraysse et al., 2006; Carrol et al, 2008). The observed discrepancy was particularly evident in the different position of the adsorption maximum between measured and calculated B adsorption envelopes in NaCl solutions, which strongly depends on the selected p$K_{>SiO^-}$ value.

The p$K_{>SiO^-}$ value that best describes the distribution of B adsorption data (p$K_{>SiO^-}$ = 11.0) may look unrealistically high compared to most values reported in the literature. However, several considerations support the validity of the value selected in this study.

It is known from several experimental and computational studies that the deprotonation constant of silanol groups ($K_{>SiO^-}$) on various silica surfaces is not unique but exhibits a range of values that are function of the silanol chemical connectivity and inter-silanol hydrogen bonding (e.g., Ong et al., 1992; Leung et al., 2009; Sulpizi et al., 2012). The deprotonation constants of silica surfaces determined by surface titration or other surface sensitive techniques are likely to be the result of the contribution of different coexisting types

533 of silanol groups (isolated, vicinal, geminal, H-bonded), each of which is characterized by a
534 specific p$K_{>SiO^-}$ value. In the case of amorphous silica and pure water, the ab-initio molecular
535 dynamics study by Pfeiffer-Laplaud et al. (2016) reported p$K_{>SiO^-}$ values equal to 8.9, 10.3
536 and 16.2 for geminal, isolated and vicinal silanols, respectively. The relative proportion of
537 silanol groups bearing different coordination and acid character depends on the interfacial
538 water structure and accessibility, which is also influenced by the nature and concentration of
539 the electrolytes (Dove and Craven, 2005; Azam et al., 2012; DelloStritto et al., 2016; Rimsza
540 et al., 2018). At the quartz/water interface, for example, the presence of both Na^+ and Cl^- ions
541 has the combined effect of weakening the silanol-silanol intrasurface H-bond network, thus
542 reducing the overall silanol acidity relative to pure water (Pfeiffer-Laplaud and Gaigeot,
543 2016).

544 Additional factors that contribute to the determination of silica surface acidity are the
545 degree of hydration of the starting solid and the concentration of the suspension. The
546 relatively high $SiO_{2(am)}$/aqueous solution ratio of our equilibrium suspension (~ 220 g/L) and
547 the small silica particle size can favor the aggregation and condensation of particles via
548 siloxane bonds (Si-O-Si) formation, despite the presence of repulsive ionic charge (cf. Iler,
549 1979). This process increases the hydrophobic character of $SiO_{2(am)}$ lowering the overall
550 surface acidity (cf. Hassanali et al., 2010).

551 The amorphous silica powder used in our study has the same origin and protocol
552 preparation as that used by Stamm et al. (2019), who determined an overall H_2O content of ~
553 8.7 weight %, corresponding to the chemical formula $SiO_2 \cdot 0.32H_2O$. As a term of
554 comparison, the value of the p$K_{>SiO^-}$ determined by Fraysse et al. (2006) for a more hydrated
555 silica ($SiO_2 \cdot 2.2H_2O$) in a NaCl 0.01 M suspension of 20g/L is equal to 7.7. The three orders
556 of magnitude difference relative to the value adopted in our modelling work indicates that the
557 original hydration of the SiO_2 surface as well as the concentration of the suspension are
558 critical factors in the determination of the acid-base properties of amorphous silica.

559 The combined effect of the above-mentioned factors expands the range of possible values
560 for silica protonation/deprotonation reaction constant. Our fitted p$K_{>SiO^-}$ value thus falls
561 within the range of the acidity constants expected for surface silanol groups and can be related
562 to a high hydrophobic character of the $SiO_{2(am)}$ suspensions. As such, this value must be
563 considered as strictly representative of the experimental conditions of this work.

564 *4.1.2 Effect of the background electrolyte on B surface speciation*

565 The striking differences in the B surface complexation behavior between the two
566 background electrolyte solutions can be explained by the distinct effect of Na^+ and Ca^{2+} ions
567 on the electrostatic properties of the $SiO_{2(am)}$/water interface. The effect of alkali and alkali-
568 earth metal ions on the silica/water interface properties is manifested by a relative increase of
569 negative surface charges (Karlsson et al., 2001; Dove and Craven, 2005) and the perturbation
570 of the interfacial water structure brought about by the adsorption of these cations (Azam et al.,
571 2012; Dewan et al., 2014; DelloStritto et al., 2016; Rimsza et al., 2018, 2019). Because of
572 their lower charge density, monovalent cations such as Na^+ promote much less negative
573 charge at the silica surface than divalent cations, such as Ca^{2+}. This difference also reflects the
574 stronger solvent-structuring character of Ca^{2+} relative to Na^+ and the consequent increased
575 H_2O ordering within the interfacial structure in $CaCl_2$ solutions (Dove and Craven, 2005).

576 The higher negative charge density developed in $CaCl_2$ solutions, the higher charge
577 screening effect operated by Ca^{2+} ions, together with the slight increase in ionic strength, are
578 expected to increase the stability of the inner-sphere configuration at the expense of the outer-
579 sphere complexes (cf. Sparks, 2003; Sverjensky and Fukushi, 2006; DelloStritto et al., 2016).
580 Our model, excluding the formation of negatively charged outer-sphere B4 complexes in
581 $CaCl_2$ solutions is, therefore, consistent with the general observations gathered from other
582 studies. In addition, the higher extent of B adsorption in $CaCl_2$ indicates that the formation of
583 B4 inner-sphere complex is stronger than in NaCl solutions of the same molality, where part
584 of the tetrahedral boron might be adsorbed as less stable outer-sphere complex. With regard to
585 the exclusion of trigonal boron from the adsorbed species, it can be as well related to the high
586 negative charge density of silica surface functional groups, requiring an increased amount of
587 excess counterions (Ca^{2+}, and also Na^+) to balance that charge (Bohinc et al., 2001; Sparks,
588 2003), thus preventing the specific adsorption of neutrally charged B3 (cf. Santos et al.,
589 2020). According to our model the negative surface charge density at the 0-plane in $CaCl_2$
590 solutions is indeed 25-100 times higher compared to NaCl solutions at pH < 8.5, where most
591 of trigonal B is adsorbed, confirming the hypothesis of B surface speciation control by the
592 surface charge and $SiO_{2(am)}$/water interface structure. In addition, note that in the NaCl
593 medium the net surface charge at the 0-plane is predicted to become positive at pH < 6.5,
594 whereas it is always negative in the $CaCl_2$ medium within the studied pH range (6-12).

595 Finally, the robustness of our model for $CaCl_2$ solutions is supported by the isotopic
596 composition of adsorbed B as a function of pH (Figs. 3 & 6), which is described by the only
597 adsorption of borate ions.

598 **4.2 Boron isotope fractionation factors between adsorbed and dissolved species**

599 The boron isotope fractionation factors calculated for the surface complexes inferred from
600 the proposed adsorption models show that high extents of fractionation are required for both
601 trigonal and tetrahedral boron species to explain our isotopic data in 0.01 M NaCl solutions.
602 For the three-species model, although with uncertainties of 2-4 ‰, the inner sphere complexes
603 of trigonal and tetrahedral boron are lighter than their dissolved counterparts by 15 ‰,
604 whereas the outer-sphere tetrahedral complex is 13 ‰ heavier than dissolved borate ions,
605 implying a fractionation of ~27 ‰ between the two adsorbed tetrahedral species. Such a large
606 difference in the isotopic composition of two adsorbed species bearing the same coordination
607 is highly unrealistic, as it would also involve a compositional difference of over 10 ‰ for the
608 same species [$>SiOB(OH)_3^-$] between solutions of NaCl and $CaCl_2$. This discrepancy cannot
609 be accounted for by the relative differences in surface charge and interfacial water structure of
610 the two suspensions. This suggests that the two-species model provides a more accurate
611 representation of B adsorption on the $SiO_{2(am)}$ surface, despite a slightly lower agreement with
612 the experimental data distribution (Fig. 6). In this case the calculated fractionation factor
613 between adsorbed and dissolved $B(OH)_3$ is equal to -16 ‰, whereas the inner-sphere B4
614 complex is 5 ‰ lighter than aqueous $B(OH)_4^-$. The fractionation factor found for the inner
615 sphere tetrahedral complex is thus consistent with that obtained for the same surface species
616 in $CaCl_2$ solutions, which is equal to -6.5 ‰.

617 For the $CaCl_2$ solutions we postulated the presence of a Ca-borate surface species formed
618 by $B(OH)_4^-$ complexation with Ca^{2+} adsorbed at the β-plane of the $SiO_{2(am)}$-water interface.
619 According to our model this surface complex should have a B isotopic composition that is
620 intermediate between the inner-sphere B4 complex and dissolved borate ion. This can be
621 explained by the weaker interaction with the charged surface and the lower degree of $B(OH)_4^-$
622 -bond distortion between the β- and d-planes relative to the 0-plane where the inner-sphere B4
623 species are formed. Note that the formation of this complex is supported by the increase of B
624 adsorption on silica gel with increasing $CaCl_2$ concentration observed by Tanifuji et al.
625 (2009).

5. Assessing the implication of adsorption reactions in the B isotopic composition of secondary silicates and siliceous organisms

This study provides new information on B isotope fractionation during the interaction of this element with amorphous silica surface sites. Because of the diffuse presence of $SiO_{2(am)}$-rich surface coatings on altered mineral surfaces, the adsorption of boron on $SiO_{2(am)}$ could contribute to its incorporation in secondary silicate minerals forming in weathering environments. Moreover, the knowledge of B adsorption mechanisms on $SiO_{2(am)}$ can help us to understand the role of this reaction in the boron uptake by growing marine siliceous organisms.

As reported by several studies, the boron adsorbed or incorporated by clay minerals and other secondary phases is generally enriched in ^{10}B, leading to negative fractionation values relative to the aqueous solutions (cf. Gaillardet and Lemarchand, 2018, Noireaux et al., 2021) and boron contents that can vary between few tens of ppm to 300 ppm or more (e.g., Hu and Gao, 2008; Williams et al., 2001, Noireaux et al., 2021), depending on the original environmental conditions. The negative fractionation values that accompany B adsorption on amorphous silica may suggest that this reaction assists the incorporation of boron in neoforming clay minerals and other SiO_2-rich weathering products. However, the comparatively small amounts of boron adsorbed at the $SiO_{2(am)}$ surface in our experiments (~2-15 ppm) may indicate that the contribution of this reaction to the fixation of boron by secondary silicates is limited.

Some observations can also be made by comparing our experimental results with the data of different siliceous materials. Reported $\delta^{11}B$ values in diatoms and radiolarians, including the diatoms from experimental cultures, fall between -5.5 and +4.5 ‰ (Ishikawa and Nakamura, 1993; Dehyle et al., 2003; Donald et al., 2020), whereas values measured in cherts from deep-sea sediments range between -9.3 and +7.7 ‰ (Kolodny and Chaussidon, 2004) and modern siliceous sponges exhibit values from +5.8 to +24.5 ‰ (de Leon, 2015).

The boron isotope fractionation between these siliceous materials and modern seawater ($\delta^{11}B_{sw}$ = 39.61 ±0.04 ‰; Foster et al., 2010) is illustrated in Fig. 7 and compared to the isotope fractionations between boron adsorbed on amorphous silica and NaCl 0.01 M solutions measured in the present study. Because the $\delta^{11}B$ data from Ishikawa and Nakamura (1993) and Kolodny and Chaussidon (2004) are not linked to any pH estimate, the calculated fractionation data reported on this plot are represented by two boxes spanning the range in

seawater pH seen today and estimated for the geological past (cf. Clayton and Byrne, 1993; Palmer et al., 1998; Pearson and Palmer, 2000; Palmer and Pearson, 2003). It should also be noted that the span of $\Delta^{11}B$ values comprised within the cherts box is affected by some uncertainty (~2 ‰) as the B isotopic composition of the oceans was likely quite different from modern seawater composition (Lemarchand et al., 2000; Greenop et al., 2017) for the analyzed samples, the age of which ranges between 70 and 100 Myr (Kolodny and Chaussidon, 2004).

On the plot of Fig. 7 the fractionation values generated by boron adsorption on $SiO_{2(am)}$ fall within or are close to the range displayed by modern sponges and the less fractionated marine cherts compositions, whereas radiolarians, diatom ooze as well as the frustules of cultured diatoms display more negative fractionation values. This comparison suggests that the B isotopic composition of marine cherts and sponge spicules could be controlled to some extent by the B adsorption reaction.

The marine cherts analyzed by Kolodny and Chaussiddon (2004) are essentially composed of microcrystalline quartz, formed via a diagenetic process from original Opal-A deposits, and have B concentrations of 44-104 ppm. Their boron concentration and isotopic compositions were presumably determined by a sequence of dissolution and reprecipitation reactions, with samples having higher B contents and heavier compositions reflecting boron incorporation from pore water with $\delta^{11}B$ of seawater, and samples with lighter composition and lower B contents indicating recrystallization from fluids containing an increasing proportion of B derived from the dissolution of the first generation of opal (Kolodny and Chaussidon, 2004). Considering the complex nature and origin of these deposits it is difficult to argue in favor of an adsorption-controlled B isotopic signature, even for the samples with heavier isotopic compositions. Nonetheless, the coprecipitation reactions leading to relatively high B concentrations could fractionate B isotopes in a very similar manner to the adsorption reaction. It has to be noted, however, that our experimental results were acquired from dilute solution of NaCl. As a consequence, the extent of fractionation caused by adsorption and co-precipitation should be measured in seawater to assess the relative impact of the two processes on the cherts B concentration and isotopic composition. A similar argument applies to the isotopic data of sponge spicules. The process of spicule synthesis involves enzyme-mediated silica polymerization and transport mechanisms across the cell membranes that could catalyze the incorporation of boron and explain the high concentrations (400-1000 ppm) measured in this form of biogenic silica compared to the inorganic adsorption reaction

691 (Schroeder et al., 2004; Wang et al., 2012; de Leon, 2015). In addition, the large range of
692 measured $\delta^{11}B$ values likely reflects the interplay of different biological and environmental
693 factors, such as taxon-specific partitioning effects, seawater Si-concentration and temperature,
694 which can significantly affect the isotopic composition of sponge siliceous skeletons (cf. de
695 Leon, 2015). Although the precise mechanisms of B incorporation into sponges are not well
696 known, these considerations suggest that the purely inorganic adsorption reaction on
697 amorphous silica has a minor role in the B uptake by sponges. This is the conclusion that we
698 can also draw by looking at the remarkably different fractionation values of B adsorbed on
699 $SiO_{2(am)}$ (-34.1 ‰ $\leq \Delta^{11}B \leq$ -22.8 ‰) and those relative to the *T. weissflogii* diatom samples (-
700 44.6 ‰ $\leq \Delta^{11}B \leq$ -40.7 ‰) cultured by Donald et al. (2020) within the same pH range. The
701 boron concentrations of these samples (0.7-3.7 ppm) are comparable to the amounts adsorbed
702 by $SiO_{2(am)}$ in NaCl solutions, but the mechanisms of silicification responsible for the
703 incorporation of B in the diatom frustules involve complex diatom metabolism and cellular
704 processes that impart a different isotopic composition to this element (cf. Martin-Jézéquel et
705 al., 2000; Kröger et al., 2000; Mejía et al., 2013; de Leon, 2015).

706 Finally, it is clear that more work is required, in particular the experimental investigation
707 of B isotope fractionation during its co-precipitation with opal as a function of pH and at
708 seawater ionic strength, to better characterize the mechanisms controlling the boron isotopic
709 signature of siliceous organisms and develop a new B-isotope proxy for marine siliceous
710 organisms.

711 ## 6. Summary and Conclusions

712 Boron adsorption on the amorphous silica surface was investigated in 0.01 M aqueous
713 solutions of NaCl and $CaCl_2$ at room temperature. The obtained adsorption envelopes and the
714 corresponding B isotope fractionation data were interpreted within the framework of the
715 triple-layer model and were found to be consistent with the formation of trigonal inner-sphere
716 [$>SiOB(OH)_2^0$] and tetrahedral inner-sphere [$>SiOB(OH)_3^-$] complexes in NaCl solutions,
717 whereas the formation of the only inner-sphere tetrahedral complex describes well most the
718 data distribution of $CaCl_2$ solutions. In the latter solutions a limited fraction of B (< 25 %)
719 might also be adsorbed as a $CaB(OH)_4^+$ complex at pH > 8 and partially explain the relative
720 increase in the measured B adsorbed fractions.

721 The calculated isotope fractionation factors between adsorbed and dissolved boron species
722 indicate that the trigonal B complex is enriched by ~16 ‰ in the light isotope (^{10}B) compared

723 to aqueous $B(OH)_3^0$, whereas the composition of the tetrahedral complex is 5 and 6.5 ‰
724 lighter than aqueous $B(OH)_4^-$ in NaCl and $CaCl_2$ solutions, respectively. The assumed
725 formation of a $CaB(OH)_4^+$ surface complex in the Ca-bearing solutions involves a B isotope
726 composition that is intermediate between that of $>SiOB(OH)_3^-$ and that of dissolved $B(OH)_4^-$
727 but likely closer to the latter. The apparent lack of formation of the trigonal B species in these
728 solutions can be attributed to the increased negative surface charge relative to NaCl fluids and
729 to changes in the local H-bond structure at the $SiO_{2(am)}$-water interface. This observation
730 indicates that changes in ionic strength and aqueous solution composition can affect the
731 amount of adsorbed B and its chemical and isotopic composition (cf. Tanifuji et al., 2009;
732 Saldi et al., 2018). In that respect, additional work to study the adsorption of boron on SiO_2 in
733 seawater would be useful.

734 This study provides a much-needed basis to better understand the isotopic composition
735 acquired by secondary silicate minerals during weathering reactions and should help to
736 improve the interpretation of the processes that govern the uptake of boron by siliceous
737 organisms and the physiological activity in which this element is directly involved, which
738 include, for example, the growth of diatom cells, their protein content and the control of the
739 frustule solubility (cf. Lewin, 1966; Lewin and Chen, 1976; Dehyle et al., 2003). Although
740 our data cannot account alone for the isotopic signatures displayed by marine siliceous
741 organisms, they allow to explain the reported weak dependence of diatom isotopic
742 compositions on seawater pH by the simultaneous adsorption and incorporation of trigonal
743 and tetrahedral boron. The determined B isotope fractionation factors between the species
744 adsorbed at the $SiO_{2(am)}$ surface and their aqueous equivalents should help to isolate the
745 contribution of other elementary processes to the B isotopic signature of opaline skeletons.
746 The development of a rigorous boron proxy of past ocean pH based on siliceous organisms
747 would require, however, the experimental investigation as a function of pH of boron isotope
748 fractionation during its co-precipitation with amorphous silica/opal.

749

750 **Acknowledgements**

751 *We thank Philippe Besson for the technical assistance during the analyses of aqueous solution at the*
752 *ICP-OES, and Alain Castillo for his help with measuring BET surfaces of amorphous silica samples.*
753 *Lucien Datas and Teresa Hungria are warmly thanked for the TEM characterization of the SiO_2*
754 *powders at the Raimond Castaing Microcharacterization Center in Toulouse. Laeticia Faure (IPGP)*
755 *is thanked for the boron extractions from the solution samples prior to boron isotope analyses by MC-*

ICP-MS. The present work was supported by the ANR project CARBORIC, the IPGP multidisciplinary program PARI and Paris–IdF region SESAME Grant no. 12015908. Finally two anonymous reviewers are thanked for their insightful comments on the manuscript.

References

Alexandre A., Meunier J. D., Colin F. and Koud J.-M. (1997). Plant impact on the biogeochemical cycle of silicon and related weathering processes. *Geochim. Cosmochim. Acta* **61**, 677–682.

Azam M. S., Weeraman C. N., and Gibbs-Davis J. M. (2012). Specific Cation Effects on the Bimodal Acid–Base Behavior of the Silica/Water Interface. *J. Phys. Chem. Lett.* **3**, 1269–1274.

Banfield J. F. and Eggleton, R. A. (1990). Analytical Transmission Electron Microscope Studies of Plagioclase, Muscovite, and K-Feldspar Weathering. *Clay Clay Miner.* **38**, 77–89.

Basile-Doelsch I., Meunier J. D. and Parron C. (2005). Another continental pool in the terrestrial silicon cycle. *Nature* **433**, 399-402.

Berka M. and Bányai I. (2001). Surface Complexation Modeling of K^+, NO_3^-, SO_4^{2-}, Ca^{2+}, F^-, Co^{2+}, and Cr^{3+} Ion Adsorption on Silica Gel. *J. Colloid Interface Sci.* **233**, 131–135.

Bohinc K., Kralj-Iglič V., and Iglič A. (2001). Thickness of electrical double layer. Effect of ion size. *Electrochim. Acta* **46**, 3033–3040.

Bousse L. and Meindl J. D. (1986). Surface potential-pH characteristics in the theory of the oxide-electrolyte interface. In *Geochemical Processes at Mineral Surfaces,* pp. 79–98. ACS Symposium Series. Edited by J. A. Davis &K. F. Hayes. American Chemical Society, Washington D. C. 683 p..

Carroll S. A., Maxwell R. S., Bourcier, W., Martin S., and Husley S. (2002). Evaluation of silica-water surface chemistry using NMR spectroscopy. *Geochim. Cosmochim. Acta* **66**, 913–926.

Carroll S. A., Roberts S. K., Criscenti L. J., and O'Day P. A. (2008). Surface complexation model for strontium sorption to amorphous silica and goethite. *Geochem. Trans.* **9**, 1–26.

Catanzaro E. J., Champion C. E., Garner E. L., Malinenko G., Sappenfeld K.M., Shields W.R. (1970). Boric acid: isotopic, and assay standard reference materials. US National Bureau of Standards Special Publication, 260, 17–70.

Charlet L. and Manceau (1994). Evidence for the neoformation of clays upon sorption of Co (II) and Ni (II) on silicates. *Geochim. Cosmochim. Acta* **58**, 2577–2582.

Chetelat B., Gaillardet J. and Chen J. (2021) Dynamic of boron in forest ecosystems traced by its isotopes: A modeling approach. *Chem. Geol.* **560**, 119994.

Cividini D., Lemarchand D., Chabaux F., Boutin R., and Pierret M. C. (2010). From biological to lithological control of the B geochemical cycle in a forest watershed (Strengbach, Vosges). *Geochim. Cosmochim. Acta* **74**, 3143–3163.

Clayton T. D. and Byrne R. H. (1993). Spectrophotometric seawater pH measurements: total hydrogen ion concentration scale calibration of *m*-cresol purple and at-sea results. *Deep Sea Res. I* **40**, 2115–2129.

Davis J. A. and Leckie J. O. (1978). Surface ionization and complexation at the oxide/water interface II. Surface properties of amorphous iron oxyhydroxide and adsorption of metal ions. *J. Colloid Interface Sci.* **67**, 90–107.

de Bussetti S. G., Ferreiro E. A., and Helmy A. K. (1995). Sorption of boron by hydrous Al-oxide. *Clay Clay Miner.* **43**, 58–62

de Leon A. (2015) The boron geochemistry of biogenic silica: Insights from marine sponges and diatoms. PhD Thesis, 151 p.. http://hdl.handle.net/1885/117239

de Leon A., Wille M., Eggins S. M., and Ellwood M. (2009). The boron geochemistry of siliceous sponges. *AGU Fall Meeting 2009 abstracts*. Abstract id. PP11C-1325.

DelloStritto M. J., Kubicki J. D., and Sofo J. O. (2016). Effect of Ions on H-Bond Structure and Dynamics at the Quartz (101)–Water Interface. *Langmuir* **32**, 11353–11365.

Dewan S., Carnevale V., Bankura A., Eftekhari-Bafrooei A., Fiorin, G., Klein M. L., and Borguet E. (2014). Structure of Water at Charged Interfaces: A Molecular Dynamics Study. *Langmuir* **30**, 8056–8065.

Deyhle A., Hodge V., and Lewin R. A. (2003) Boron in diatoms. *PSA Abstracts: J. Phycol.* Abstract n. 33, p.12.

Dietzel M. (2002) Interaction of polysilicic and monosilicic acid with mineral surfaces. In: Water- Rock Interaction. Stober I. and Bucher K. Eds. Springer -Science+Business Media. pp. 207¬235.

Doherty (2010). PEST. Model-independent parameter estimation. User Manual. 5th edition. Watermark Numerical Computing. Web: http://www.pesthomepage.org.

Donald H. K., Foster G. L., Fröhberg N., Swann G. E. A., Poulton A., Moore C. M., and Humphreys M. P. (2020). The pH dependency of the boron isotopic composition of diatom opal (Thalassiosira weissflogii). *Biogeosciences* **17**, 2825-2837. https://doi.org/10.5194/bg-17-2825-2020.

Dove P. M. and Craven C. M. (2005). Surface charge density on silica in alkali and alkaline earth chloride electrolyte solutions. *Geochim. Cosmochim. Acta* **69**, 4963–4970.

Drees L. R., Wilding L. P., Smeck N. E., and Senkayi A. L. (1989). Silica in soils: Quartz and disordered polymorphs. In: Dixon J. B. and Weed S. B. (Eds.), Minerals in soil environments. Soil Sci. Soc. Am. Book Series No. 1, Madison, Wisconsin, USA, pp. 913–974.

Eggins S. M., Ellwood M., McCulloch M. and Kelly M. (2004). Silica sponges – archives of paleoseawater pCO_2? *Research School of Earth Sciences. Annual Report, The Australian National University*.

Farmer J. R., Branson O., Uchikawa J., Penman D. E., Hönisch B., and Zeebe R. E. (2019). Boric acid and borate incorporation in inorganic calcite inferred from B/Ca, boron isotopes and surface kinetic modeling. *Geochim. Cosmochim. Acta* **244**, 229–247.

Farmer V. C., Delbos E. and Miller J. D. (2005) The role of phytolith formation and dissolution in controlling concentrations of silica in soil solutions and streams. *Geoderma* **127**, 71–79.

Foster G. L., Pogge von Strandmann P. A. E. and Rae J. W. B. (2010) Boron and magnesium isotopic composition of seawater. *Geochem. Geophys. Geosyst.* **11**(8), Q08015.

Fraysse F., Pokrovsky O. S., Schott J., and Meunier J.-D. (2006). Surface properties, solubility and dissolution kinetics of bamboo phytoliths. *Geochim. Cosmochim. Acta* **70**, 1939–1951. http://doi.org/10.1016/j.gca.2005.12.025

Gaillardet J. and Lemarchand D. (2018). Boron in weathering environment. In: Marschall H. and Foster G. (Eds) "Boron Isotopes, The fifth element". Springer International Publishing. pp. 163–188.

Goldberg S. (1997). Reactions of boron with soils. *Plant and Soil* **193**, 35–48.

Goldberg S. (2005). Prediction of boron adsorption by field samples of diverse structure. *Soil Sci. Soc. Am. J.* **69**, 1379–1388.

Goldberg S. and Forster H. S. (1991). Boron sorption on calcareous soils and reference calcites. *Soil Science* **152**, 304–310.

Goldberg S., Forster H. S., and Heick E. L. (1993) Boron adsorption mechanisms on oxides, clay minerals and soils inferred from ionic strength effects. *Soil Sci. Soc. Am. J.* **57**, 704–708.

Goldberg, S., & Glaubig, R. A. (1986). Boron Adsorption and Silicon Release by the Clay Minerals Kaolinite, Montmorillonite, and Illite. *Soil Sci. Soc. Am. J.* **50**, 1442–1448.

Greenop R., Hain M. P., Sosdian S. M., Oliver K. I. C., Goodwin P., Chalk T. B., et al. (2017). A record of Neogene seawater $\delta^{11}B$ reconstructed from paired $\delta^{11}B$ analyses on benthic and planktic foraminifera. *Clim. Past* **13**, 149–170.

Gustafsson J. P. (2012). Visual MINTEQ (v3.1). A Windows version of MINTEQA2. http://vminteq.lwr.kth.se/

Hassanali A. A., Zhang H., Knight C., Shin Y. K., and Singer S. J. (2010). The Dissociated Amorphous Silica Surface: Model Development and Evaluation. *J. Chem. Theory Comput.* **6**, 3456–3471.

Hellmann R., Wirth R., Daval D., Barnes J.-P., Penisson J.-M., Tisserand D. et al. (2012). Unifying natural and laboratory chemical weathering with interfacial dissolution–reprecipitation: A study based on the nanometer-scale chemistry of fluid–silicate interfaces. *Chem. Geol.* **294-295**, 203–216.

869 Hochella M. F. Jr. and Banfield J. F. (1995) Chemical weathering of silicates in nature: A
870 microscopic perspective with theoretical considerations. In: Chemical weathering rates of
871 silicate minerlas. *Rev, Mineral.* **31**, pp. 353–406.

872 Hu Z. and Gao S. (2008). Upper crustal abundances of trace elements: A revision and update.
873 *Chem. Geol.* **253**, 205–221.

874 Icenhower J. P. and Dove P. M. (2000) Water behavior at silica surfaces. In *Adsorption on*
875 *silica surfaces,* pp. 277–295. Edited by E. Papirer. Marcel Dekker, Inc., New York, 753 p..

876 Iler R. (1979). The chemistry of silica. Solubility, polymerization, colloid and surface
877 properties and biochemistry. Wiley & Sons, 896 p..

878 Ishikawa T. and Nakamura E. (1993). Boron isotope systematics of marine sediments. *Earth*
879 *Planet. Sci. Lett.* **117**, 567–580.

880 Johnson C. M., Beard B. L. and Albarède F. (2004) Overview and general concepts. *Rev.*
881 *Mineral. Geochem.* **55**, 1-24.

882 Johnson J. W., Oelkers E. H., and Helgeson H. C. (1992) SUPCRT92: A software package for
883 calculating the standard molal thermodynamic properties of minerals, gases, aqueous
884 species and reactions from 1 to 5000 bar and 0 to 1000 °C. *Comput. Geosci.* **18**, 899–947.

885 Kaczmarek K., Nehrke G., Misra S., Bijma J., and Elderfield H. (2016). Investigating the
886 effects of growth rate and temperature on the B/Ca ratio and $\delta^{11}B$ during inorganic calcite
887 formation. *Chem. Geol.***421**, 81–92. http://doi.org/10.1016/j.chemgeo.2015.12.002

888 Karlsson M., Craven C., Dove P. M., and Casey, W. H. (2001). Surface Charge
889 Concentrations on Silica in Different 1.0 M Metal-Chloride Background Electrolytes and
890 Implications for Dissolution Rates. *Aquat. Geochem.*, **7**, 13–32.

891 Keren R., Bingham F. T. and Rhoades J. D. (1985). Plant uptake of boron as affected by
892 boron distribution between liquid and solid phases in soil. *Soil Sci. Soc. Am. J.* **49**, 297–
893 302.

894 Kim Y. and Kirkpatrick, R. J. (2006). ^{11}B NMR investigation of boron interaction with
895 mineral surfaces: Results for boehmite, silica gel and illite. *Geochim. Cosmochim. Acta*,
896 **70**, 3231–3238.

897 Klochko K., Kaufman A. J., Yao W., Byrne R. H. and Tossell, J. A. (2006) Experimental
898 measurement of boron isotope fractionation in seawater. *Earth Planet. Sci. Lett*. **248**, 276-
899 285.

900 Kolodny Y. and Chaussidon M. (2004). Boron isotopes in DSDP cherts: fractionation and
901 diagenesis. *Geochemical Investigations in Earth and Space Science: A tribute to I. R.*
902 *Kaplan.* The Geochemical Society, Publication No. 9, 2004, 14 p..

903 Kosmulski M. (1994). Co-adsorption of mono- and multivalent ions on silica and alumina.
904 *Ber. Bunsenges. Phys. Chem.* **98**, 1062–1067.

Kosmulski M. (1996). Adsorption of cadmium on alumina and silica: Analysis of the values of stability constants of surface complexes calculated for different parameters of triple layer model. *Colloids Surf.* **117**, 201–214.

Kosmulski M. (1997). The Effect of the Ionic Strength on the Adsorption Isotherms of Nickel on Silica. *J. Colloid Interface Sci.* **190**, 212–223.

Kosmulski M., Eriksson P., Gustafsson J., and Rosenholm J. B. (1999). Specific Adsorption of Nickel and ζ Potential of Silica at Various Solid-to-Liquid Ratios. *J. Colloid Interface Sci.*, **220**, 128–132.

Kröger N., Deutzmann R., Bergsdorf C., and Sumper M. (2000). Species-specific polyamines from diatoms control silica morphology. *P. Natl Acad. Sci. USA* **97**, 14133–14138.

Lee S. Y. and Gilkes R. J. (2005). Groundwater geochemistry and composition of hardpans in southwestern Australian regolith. *Geoderma* **126**, 59–84.

Lemarchand D., Cividini D., Turpault M.-P. and Chabaux F. (2012) Boron isotopes in different grain size fractions: Exploring past and present water-rock interactions from two soil profiles (Strengbach, Vosges Mountains). *Geochim. Cosmochim. Acta* **98**, 78–93.

Lemarchand D. and Gaillardet J. (2006) Transient features of the erosion of shales in the Mackenzie basin (Canada), evidences from boron isotopes. *Earth Planet. Sci. Lett*. **245**, 174-189.

Lemarchand D., Gaillardet J., Lewin E., and Allègre C. J. (2000). The influence of rivers on marine boron isotopes and implications for reconstructing past ocean pH. *Nature* **408**, 951–954.

Lemarchand E., Schott J. and Gaillardet, J. (2005) Boron isotopic fractionation related to boron sorption on humic acid and the structure of surface complexes formed. *Geochim. Cosmochim. Acta* **69**, 3519-3533.

Lemarchand E., Schott J. and Gaillardet, J. (2007) How surface complexes impact boron isotope fractionation: Evidence from Fe and Mn oxides sorption experiments. *Earth Planet. Sci. Lett.* **260**, 277-296.

Leung K., Nielsen I. M. B., and Criscenti L. J. (2009). Elucidating the Bimodal Acid−Base Behavior of the Water−Silica Interface from First Principles. *J. Am. Chem. Soc.*, **131**, 18358–18365. http://doi.org/10.1021/ja906190t

Lewin J. (1966). Boron as a growth requirement for diatoms. *J. Phycol.* **2**, 160–163. http://doi.org/10.1111/j.1529-8817.1966.tb04616.x

Lewin J. and Chen C.-H. (1976). Effects of boron deficiency on the chemical composition of a marine diatom. *J. Exp. Bot.* **27**, 916–921.

Liu Y. and Tossell J. A. (2005). Ab initio molecular orbital calculations for boron isotope fractionations on boric acids and borates. *Geochim. Cosmochim. Acta* **69**, 3995–4006.

Louvat P., Gaillardet J., Paris G. and Dessert C. (2011) boron isotope ratios of surface waters in Guadeloupe, Lesser Antilles. *Applied Geochem.* **26**, S76–S79.

Louvat P., Moureau J., Paris G., Bouchez J., Noireaux J., Gaillardet J. (2014). A fully automated direct injection nebulizer (d-DIHEN) for MC-ICP-MS isotope analysis: application to boron isotope ratio measurements. *J. Anal. Atom. Spectrom.* **29**, 1698-1707.

Louvat, P., Tharaud, M., Buisson, M., Rollion-Bard, C., and Benedetti, M. F. (2019). µ-dDIHEN: a new micro-flow liquid sample introduction system for direct injection nebulization in ICP-MS, *J. Anal. At. Spectrom.* **34** 1553-1563.

Martin-Jézéquel V., Hildebrand M., and Brzezinski M. A. (2000). Silicon metabolism in diatoms: Implications for growth. *J. Phycol.* **36**, 821–840.

Mejía L. M., Isensee K., Méndez-Vicente A., Pisonero J., Shimizu N., et al. (2013). B content and Si/C ratios from cultured diatoms (*Thalassiosira pseudonana* and *Thalassiosira weissflogii*): Relationship to seawater pH and diatom carbon acquisition. *Geochim. Cosmochim. Acta* **23**, 322–337.

Nir O., Vengosh A., Harkness J. S., Dwyer G.S., Lahav O. (2015) Direct measurement of the boron isotope fractionation factor: reducing the uncertainty in reconstructing ocean paleo-pH. *Earth Planet. Sci. Lett*. **414**, 1-5.

Noireaux J., Mavromatis V., Gaillardet J., Schott J., Montouillout V., Louvat P., Rollion-Bard C. and Neuville D. R. (2015) Crystallographic control on the boron isotope pH proxy. *Earth Planet. Sci. Lett*. **430**, 398-407.

Noireaux J., Sullivan P. L., Gaillardet J., Louvat P., Steinhoefel G., Brantley S. L. (2021). Developing boron isotopes to elucidate weathering in the critical zone. *Chem. Geol.* **559**, 119900.

Nugent M. A., Brantley S. L., Pantano C. G. and Maurice P. A. (1998). The influence of natural mineral coatings on feldspar weathering. *Nature* **39**, 588–591.

Ong S., Zhao X., and Eisenthal K. B. (1992). Polarization of water molecules at a charged interface: second harmonic studies of the silica/water interface. *Chem. Phys. Lett.* **191**, 327–335.

Palmer M. R., Pearson P. N. and Cobb S. J. (1998). Reconstructing Past Ocean pH-Depth Profiles. *Science* **282**, 1468–1471.

Palmer M. R. and Pearson P. N. (2003). A 23,000-year record of surface water pH and P_{CO2} in the western equatorial Pacific Ocean. *Science* **300**, 480–482.

Palmer M. R., Spivack A. J., and Edmond J. M. (1987). Temperature and pH controls over isotopic fractionation during adsorption of boron on marine clay. *Geochim. Cosmochim. Acta* **51**, 2319–2323.

Peak D., Luther III G. W., and Sparks D. L. (2003) ATR-FTIR spectroscopic studies of boric acid adsorption on hydrous ferric oxide. *Geochim. Cosmochim. Acta* **67**, 2551–2560.

Pearson P. N. and Palmer M. R. (2000). Atmospheric carbon dioxide concentrations over the past 60 million years. *Nature* **406**, 695–699.

Persello J. (2000) Surface and Interface Structure of Silicas. In *Adsorption on silica surfaces,* pp. 297–342. Edited by E. Papirer. Marcel Dekker, Inc., New York, 753 p..

Pfeiffer-Laplaud M. and Gaigeot M.-P. (2016). Adsorption of Singly Charged Ions at the Hydroxylated (0001) α-Quartz/Water Interface. *J. Phys. Chem. C* **120**, 4866–4880.

Pfeiffer-Laplaud M., Gaigeot M.-P., and Sulpizi M. (2016). pKa at Quartz/Electrolyte Interfaces. *J. Phys Chem. Lett.* **7**, 3229–3234.

Pivovarov S. (2010). Diffuse sorption modeling: Ionic adsorption on silica. *J. Colloid Interface Sci*. **352**, 158–162.

Rimsza J. M., Jones R. E., and Criscenti L. J. (2018). Interaction of NaOH solutions with silica surfaces. *J. Colloid Interf. Sci.* **516**, 128–137.

Rimsza J. M., Jones R. E., and Criscenti L. J. (2019). Mechanisms of Silica Fracture in Aqueous Electrolyte Solutions. *Front. Mater.* **6**: 79.

Rose E. F., Chaussidon M., and France-Lanord C. (2000) Fractionation of boron isotopes during erosion processes: The example of Himalayan rivers. *Geochim. Cosmochim. Acta* **64**, 397–408.

Rustad J. R., Bylaska E. J., Jackson V. E., and Dixon D. A. (2010). Calculation of boron-isotope fractionation between $B(OH)_3$(aq) and $B(OH)_4^-$(aq). *Geochim. Cosmochim. Acta* **74**, 2843–2850.

Saccone L., Conley D. J., Koning E., Sauer D., Sommer M., et al. (2007) Assessing the extraction and quantification of amorphous silica in soils of forest and grassland ecosystems. *Eur. J. Soil Sci.* **58**, 1446–1459.

Sah R. N. and Brown P. H. (1997) Boron determination—a review of analytical methods. *Microchem. J.* **56**, 285-304.

Sahai N. and Sverjensky D. A. (1997a). Evaluation of internally consistent parameters for the triple-layer model by the systematic analysis of oxide surface titration data. *Geochim. Cosmochim. Acta* **61**, 2801–2826.

Sahai N. and Sverjensky D. A. (1997b). Solvation and electrostatic model for specific electrolyte adsorption. *Geochim. Cosmochim. Acta* **61**, 2827–2848.

Saldi G. D., Noireaux J., Louvat P., Faure L., Balan E., Schott J., and Gaillardet J. (2018). Boron isotopic fractionation during adsorption by calcite – Implication for the seawater pH proxy. *Geochim. Cosmochim. Acta* **240**, 255–273.

Santos dos P., Goldberg S., and Costa da A. C. S. (2020). Modeling boron adsorption on five soils before and after removal of organic matter. *Sci. Agric.* **77**, n.4: e20180023.

Schindler M., Durocher J. L., Abdu Y., and Hawthorne F. C. (2009). Hydrous Silica Coatings: Occurrence, Speciation of Metals, and Environmental Significance. Environ. Sci. Technol. 43, 8775–8780.

Schindler M. and Hochella M. F. Jr. (2015). Soil memory in mineral surface coatings: Environmental processes recorded at the nanoscale. Geology 43, 415–418.

Schindler M. and Singer D. (2017). Mineral surface coatings: Environmental records at the nanoscale. Elements 13, 159–164.

Schindler P. W. and Stumm W. (1987) The surface chemistry of oxides, hydroxides, and oxide minerals. In: *Aquatic Surface Chemistry*. Stumm W. (ed), John Wiley, New York, pp. 83-110.

Schott J., Pokrovsky O.S., Spalla O., Devreux F., Gloter A., Mielczarski J.A. (2012) Formation growth and transformation of leached layers during silicate minerals dissolution: The example of wollastonite. *Geochim. Cosmochim. Acta* **98**, 258–281.

Schwarcz H. P., Agyei E. K., McMullen C. C. (1969) Boron isotopic fractionation during clay adsorption from Sea-Water. Earth Planet Sci Lett 6, 1–5.

Schröder H.-C., Perovic-Ottstadt S., Rothenberger M., Wiens M., Schwertner H., Batel R., et al. (2004). Silica transport in the demosponge *Suberites domuncula*: fluorescence emission analysis using the PDMPO probe and cloning of a potential transporter. *Biochem. J* **381**, 665–673.

Sparks D. L. (2003). Environmental Soil Chemistry. 2nd Edition. Academic Press, Elsevier Science. 352 p..

Spivack A. J., Palmer M. R., Edmond J. M. (1987) The sedimentary cycle of the boron isotopes. *Geochim. Cosmochim. Acta* **51**, 1939–1949.

Stamm F. M., Zambardi T., Chmeleff J., Schott J., Blanckenburg von F., and Oelkers, E. H. (2019). The experimental determination of equilibrium Si isotope fractionation factors among $H_4SiO_4°$, $H_3SiO_4^-$ and amorphous silica ($SiO_2 \cdot 0.32\ H_2O$) at 25 and 75 °C using the three-isotope method. *Geochim. Cosmochim. Acta* **255**, 49–68.

Sulpizi M., Gaigeot M.-P., and Sprik M. (2012). The Silica–Water Interface: How the Silanols Determine the Surface Acidity and Modulate the Water Properties. *J. Chem. Theory Comput.* **8**, 1037–1047.

Sverjensky D. A. (2001). Interpretation and prediction of triple-layer model capacitances and the structure of the oxide-electrolyte-water interface. *Geochim. Cosmochim. Acta* **65**, 3643–3655.

Sverjensky D. A. (2006). Prediction of the speciation of alkaline earths adsorbed on mineral surfaces in salt solutions. *Geochim. Cosmochim. Acta* **70**, 2427–2453.

Sverjensky D. A. and Fukushi K. (2006). Anion Adsorption on Oxide Surfaces: Inclusion of the Water Dipole in Modeling the Electrostatics of Ligand Exchange. *Environ. Sci. Technol.* **40**, 263–271.

Tanifuji K., Seike Y., and Okumura, M. (2009). Removal of Borate-Boron from Aqueous Solution Using Its Adsorption to Silica Gel. *Buseki Kagaku* **58**, 767-770.

Thiry M., Milnes A. R., Rayot V. and Simon-Coinçon R. (2006). Interpretation of palaeoweathering features and successive silicifications in the Tertiary regolith of inland Australia. *J. Geol. Soc.* **163**, 723–736.

1056 Vogl J. and Rosner M. (2011) Production and Certification of a Unique Set of Isotope and
1057 Delta Reference Materials for Boron Isotope Determination in Geochemical,
1058 Environmental and Industrial Materials. Geost. Geoanal. Res., 36, 161-175.

1059 Vrieling E. G., Gieskes W. W. C., and Beelen T. P. M. (1999). Silicon deposition in diatoms:
1060 control by the pH inside the silicon deposition vesicle. *J. Phycol.* **35**, 548–559.

1061 Wang X., Schröder H. C., Wiens M., Schloßmacher, U., and Muller W. E. G. (2012).
1062 Biosilica: Molecular Biology, Biochemistry and Function in Demosponges as well as its
1063 Applied Aspects for Tissue Engineering. *Adv. Mar. Biol.* **62**, 231–271.

1064 Williams L. B., Hervig R. L., Holloway J. R., Hutcheon I. (2001) Boron isotope geochemistry
1065 during diagenesis. Part II. Applications to organic-rich sediments. *Geochim. Cosmochim.*
1066 *Acta* **65**, 1783–1794.

1067 Yates D. E., Levine S., and Healy T. W. (1974). Site-binding model of the electrical double
1068 layer at the oxide/water interface. *J. Chem. Soc. Farad. T1* **70**, 1807–1818.

1069 Zhu C., Veblen D. R., Blum A. E. and Chipera S. J. (2006). Naturally weathered feldspar
1070 surfaces in the Navajo Sandstone aquifer, Black Mesa, Arizona: Electron microscopic
1071 characterization. *Geochim. Cosmochim. Acta* **70**, 4600–4616.

1072 Zhuravlev L. T. (2000). The surface chemistry of amorphous silica. Zhuravlev model. *Colloid*
1073 *Surface A* **173**, 1–38.

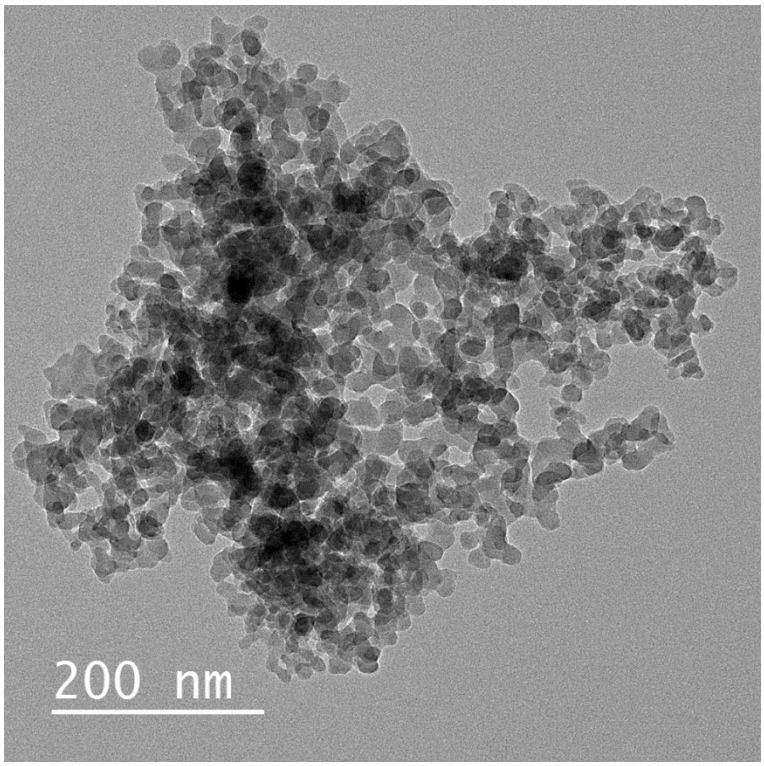

Figure 1. TEM image of the starting amorphous silica powder used for the study of boron adsorption.

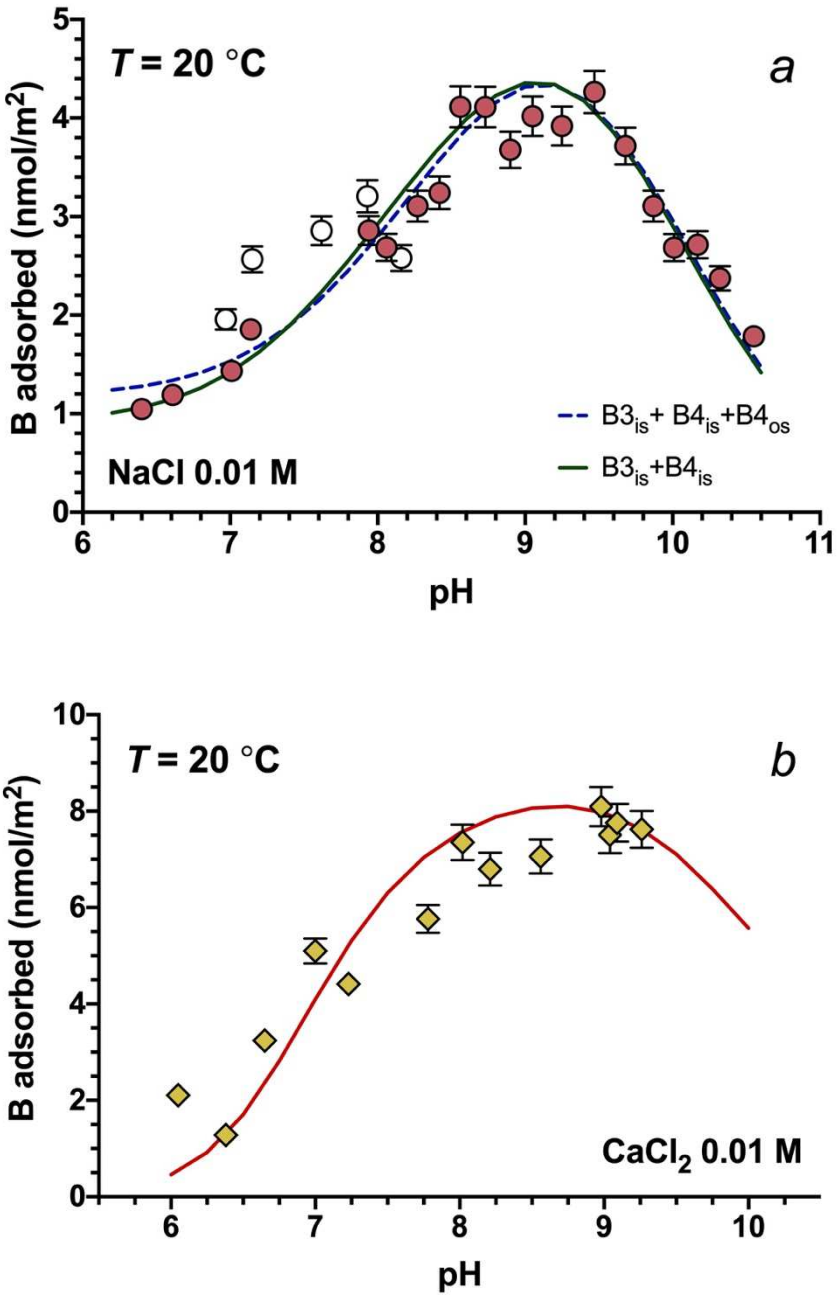

Figure 2. Boron adsorption on $SiO_{2(am)}$ as a function pH at 20 °C in 0.01 M NaCl **(a)** and 0.01 $CaCl_2$ **(b)** along with the predictions of the triple-layer model adopted to quantify the intrinsic stability constants of the surface complexes forming at the $SiO_{2(am)}$-fluid interface (lines drawn through the symbols). The empty circles in (a) are the data excluded from the fitting procedure. The error bars of the datapoints take into account the average analytical error in the determination of B concentrations (± 1%) and the uncertainty inherent in the BET specific surface area measurements (± 5%).

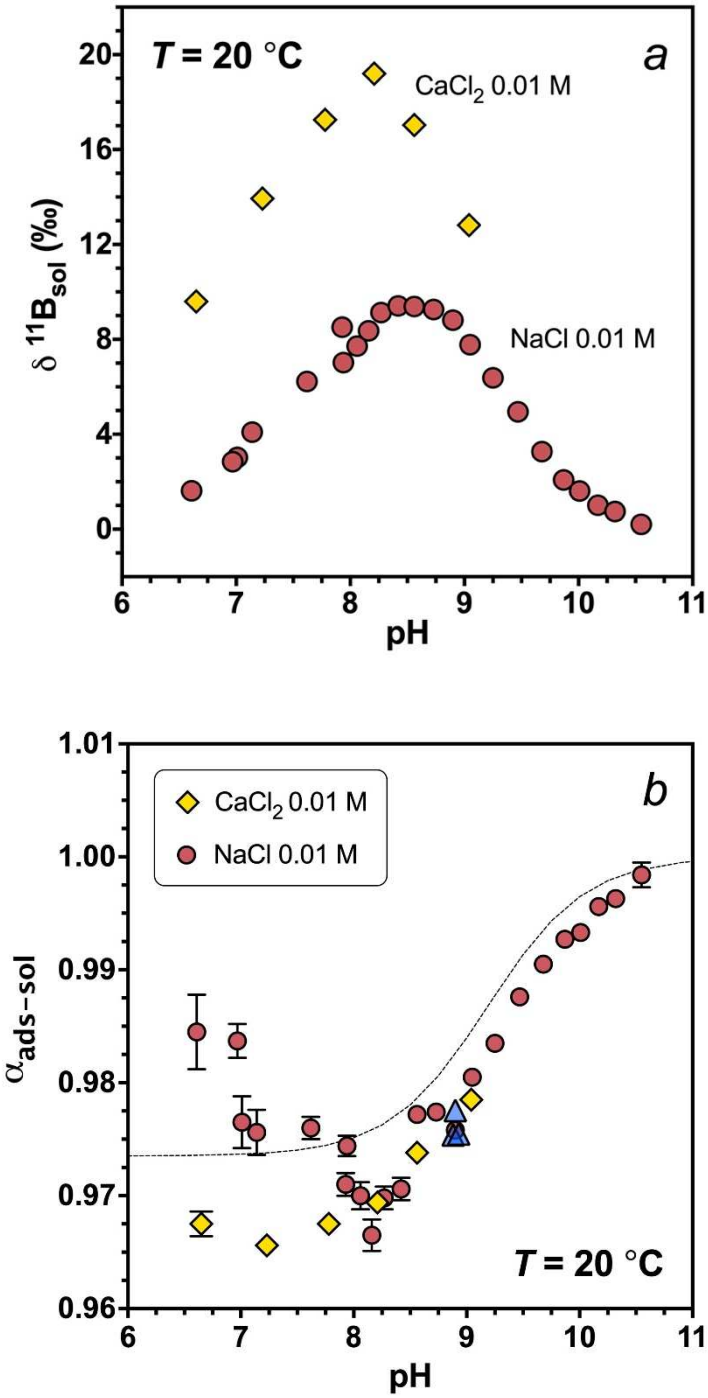

Figure 3. Boron isotopic composition of the aqueous samples upon B adsorption at the $SiO_{2(am)}$ surface in NaCl and $CaCl_2$ solutions (a) and the corresponding B isotopic fractionation factors between the amorphous silica surface and the aqueous solution (b). Blue triangles in (b) represent a 5-48 hrs series showing that the measured variation of the isotope fractionation values is within the data uncertainties. The black dashed line represents the isotopic composition of the borate ion for $\alpha_{3\text{-}4} = 1.027$ at the given ionic strength.

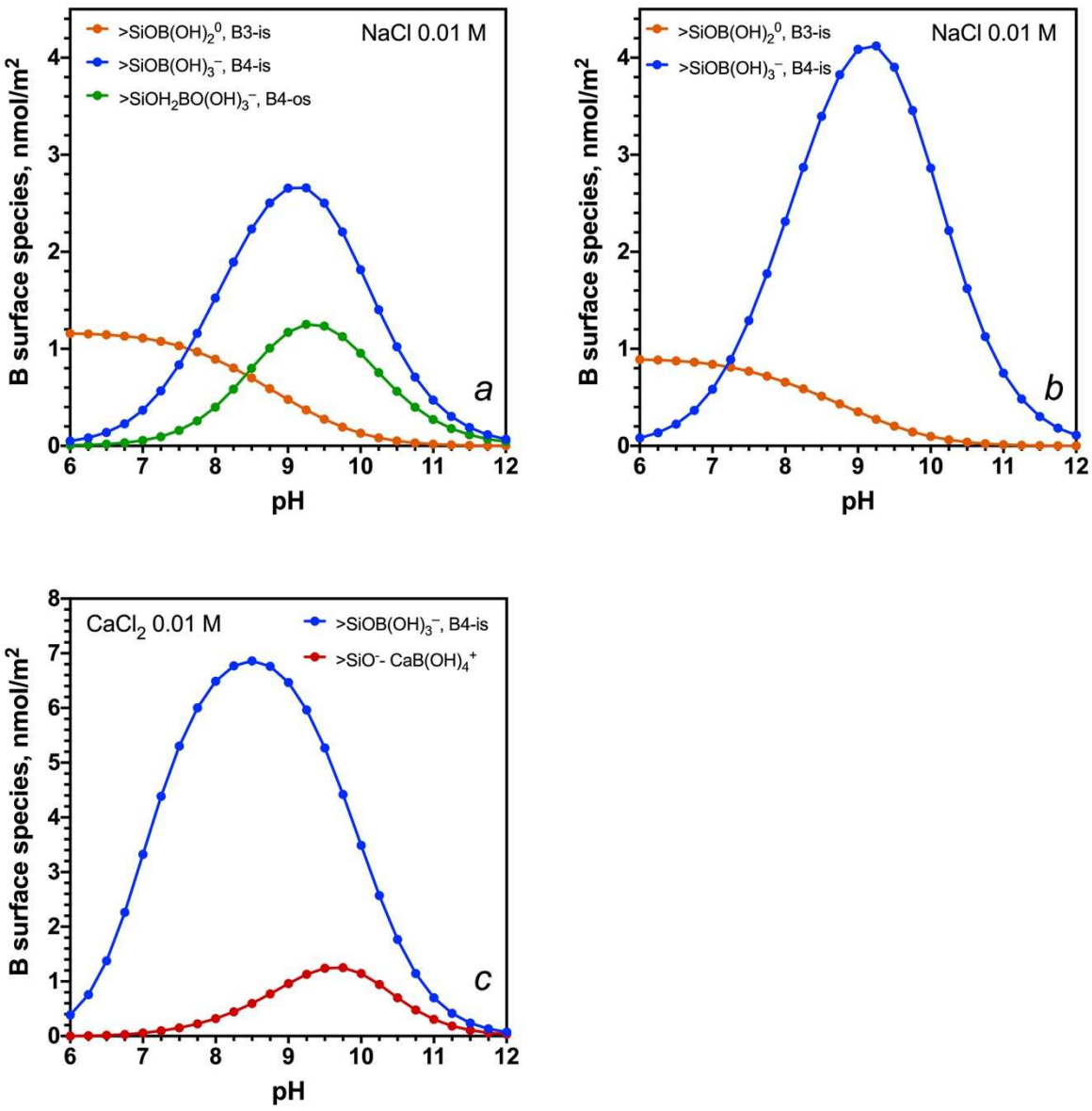

Figure 4. pH-dependent surface concentration of the B complexes formed on the $SiO_{2(am)}$ surface in 0.01 M NaCl and $CaCl_2$ aqueous solutions according to the models proposed to describe the measured B adsorption envelopes. a) Three-species model for NaCl solutions including a B4 outer-sphere complex (B4-os). b) Two-species model for NaCl solutions considering only B3 and B4 inner-sphere complexes (B3-is, B4-is). c) Distribution of the surface species used to describe B adsorption in solutions of $CaCl_2$. The reported surface species distributions are representative of the following conditions: suspension concentration = 220 g/l; $[B]_0$ = 0.463 mmol/kg.

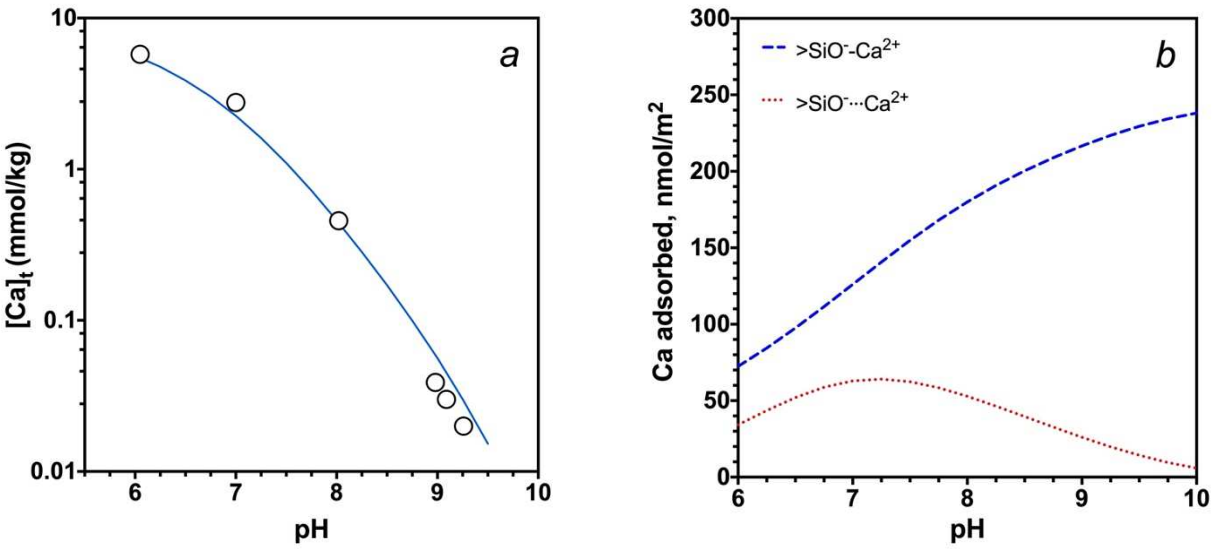

Figure 5. Modelling of Ca adsorption at the $SiO_{2(am)}$ surface. (a) Comparison between measured Ca concentrations (circles) and the Ca concentrations predicted by the model of Ca adsorption adopted in this study. (b) pH-dependent distribution of the two Ca surface species assumed to form at the $SiO_{2(am)}$/fluid interface in $CaCl_2$ aqueous solutions.

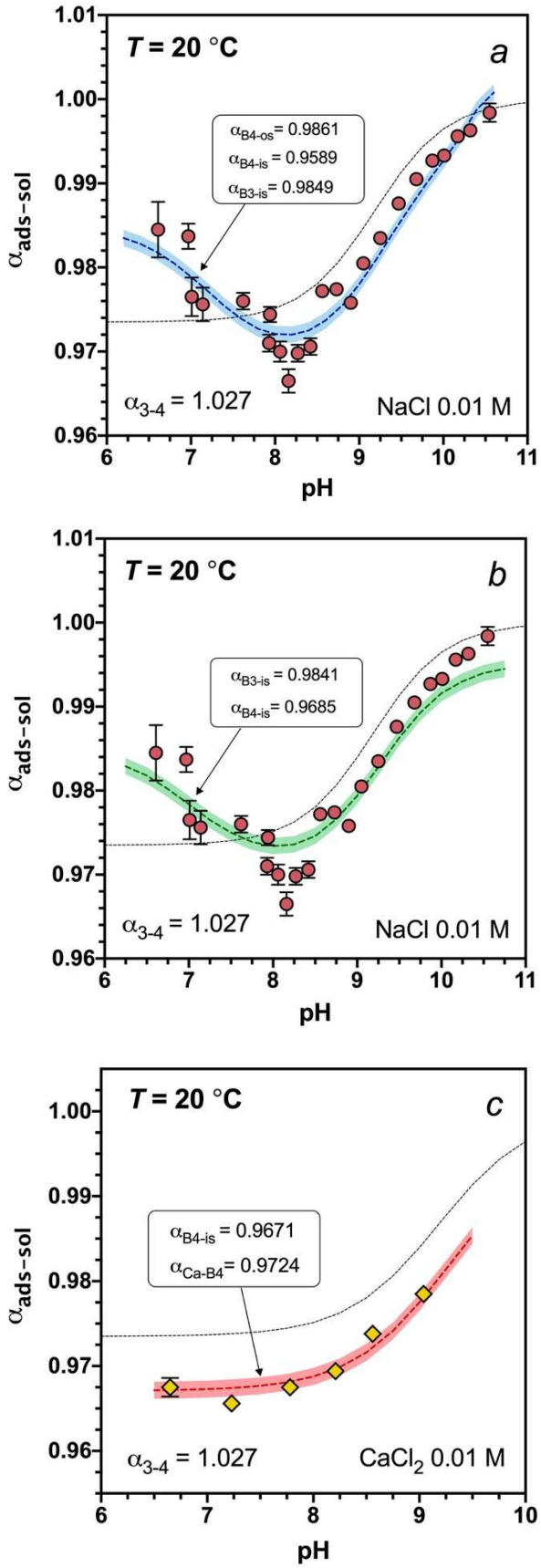

Figure 6. Modelling of the B isotopic fractionation factor between $SiO_{2(am)}$ and aqueous solutions for NaCl 0.01 M (a & b) and $CaCl_2$ 0.01 M (c). The model in (a) represent the least

square fit of the three-species model, whereas (b) illustrates the results of the fit relative to the two-species model (only inner-sphere complexes are considered). The black dashed line on the three plots represents the isotopic composition of the borate ion for the given ionic strength and for $\alpha_{3\text{-}4} = 1.027$.

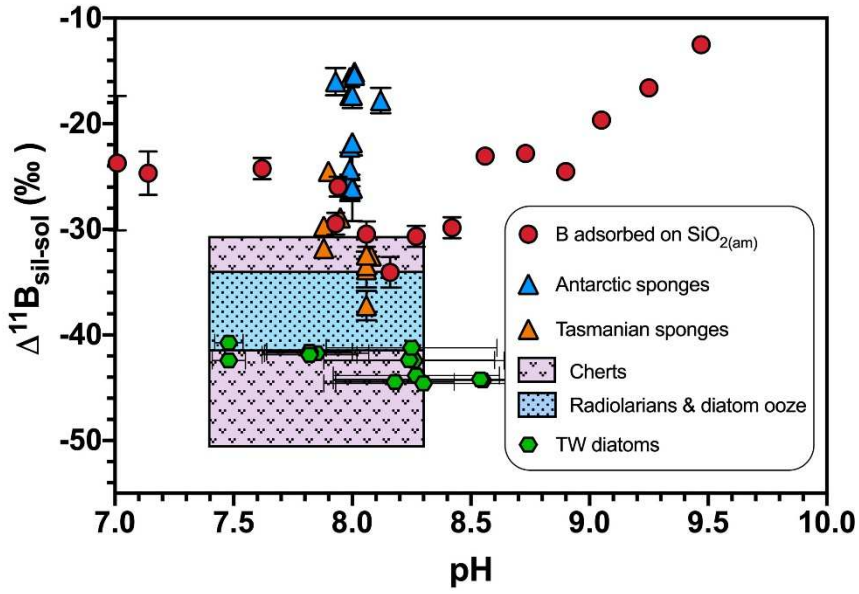

Figure 7. Boron isotopic fractionation ($\Delta^{11}B$) of marine siliceous materials and of the fraction adsorbed onto $SiO_{2(am)}$ in 0.01 M NaCl solutions as a function of pH. The $\Delta^{11}B$ values of marine samples are calculated from the boron isotopic composition ($\delta^{11}B$) provided by literature studies relative to the same value of modern seawater B isotope composition ($\delta^{11}B_{sw}$ = 39.61 ±0.04 ‰), except for the diatoms samples for which $\Delta^{11}B$ were calculated from the seawater composition ($\delta^{11}B_{sw}$ = 38.8 ±0.19 ‰) provided by Donald et al. (2020). The B isotopic composition of siliceous sponges (triangles) are taken from de Leon (2015), the $\delta^{11}B$ of cherts from Kolodny and Chaussidon (2004) and those of radiolarians and diatom ooze and TW diatoms are provided, respectively, by Ishikawa and Nakamura (1993) and Donald et al. (2020). Note that for cherts, radiolarians and diatom ooze the original seawater pH is not known. For this reason, the calculated fractionation values were included into boxes encompassing estimated and modern seawater pH-range (cf. Clayton and Byrne, 1993; Pearson and Palmer, 2000).

Table 1. Summary of the surface complexation reactions used in the present study to characterize the adsorption of boron on the amorphous silica surface in solutions of NaCl and $CaCl_2$. The values of the log K^0_{int} determined in this study refer to a single site triple-layer model (TLM) and were obtained with the following model parameters: C_1 = 2.2 F/m^2; C_2 = 0.05 F/m^2; $>SiOH^0$ site density = 4.6 nm^{-2}.

Surface reaction	$Log\ K^0_{int}$ (25 °C. $I = 0$)	Source
1. $>SiOH^0 = >SiO^- + H^+$	-11.0	This study
2. $>SiOH^0 + H^+ => SiOH_2^+$	2.3	Schindler and Stumm (1987)
3. $>SiOH^0 + Na^+ = >SiO^- - Na^+ + H^+$	-7.24	Kosmulski (1997)
4. $>SiOH^0 + H^+ + Cl^- = >SiOH_2^+ - Cl^-$	-6.4	Kent et al. (1988)
5. $>SiOH^0 + Ca^{2+} = >SiO^- - Ca^{2+} + H^+$	-3.8 ± 0.4	This study
6. $>SiOH^0 + Ca^{2+} = >SiO^- \cdots Ca^{2+} + H^+$	-6.5± 0.5	This study

Table 2. Summary of the B adsorption experiments on $SiO_{2(am)}$ conducted in NaCl 0.01 M aqueous solutions.

run #	pH	$SiO_{2(am)}$	Solution	$[B]_0$	$\Delta[B]$	% B_{ads}	SSA	B_{ads}	B_{ads}	[Si]
		g	g	ppm	ppm		m^2/g	µg/g	nmol/m^2	mmol/kg
ASB#06	6.40	5.132	25.984	4.556	-0.367	8.1	164.1	1.86	1.05	13.43
SB-01	6.61	5.505	25.015	4.843	-0.521	10.7	183.9	2.37	1.19	5.31
SB-03	6.97	5.494	25.014	4.831	-0.855	17.7	183.9	3.89	1.96	3.55
SB-02	7.01	5.509	25.075	4.818	-0.627	13.0	183.9	2.85	1.44	3.77
SB-04	7.14	5.496	25.077	4.811	-0.808	16.8	183.9	3.69	1.85	2.60
ASB#07	7.15	5.374	25.636	4.591	-0.955	20.8	164.1	4.55	2.57	36.47
SB-05	7.62	5.503	25.133	4.798	-1.243	25.9	183.9	5.68	2.86	2.40
SB-06	7.93	5.499	25.242	4.774	-1.388	29.1	183.9	6.37	3.20	2.88
SB-07	7.94	5.519	25.299	4.647	-1.265	27.2	187.6	5.80	2.86	1.88
SB-08	8.06	5.497	26.063	4.506	-1.150	25.5	187.6	5.45	2.69	2.07
SB-09	8.16	5.530	25.401	4.615	-1.139	24.7	187.6	5.23	2.58	1.95
SB-10	8.27	5.562	25.456	4.596	-1.377	30.0	187.6	6.30	3.11	2.02
SB-11	8.42	5.500	25.131	4.536	-1.439	31.7	187.6	6.57	3.24	2.62
SB-12	8.56	5.533	25.023	4.505	-1.845	41.0	187.6	8.35	4.12	1.98
SB-13	8.73	5.531	25.102	4.502	-1.837	40.8	187.6	8.34	4.11	2.35
SB-14	8.90	5.520	25.050	4.551	-1.644	36.1	187.6	7.46	3.68	2.13
SB-15	9.05	5.536	25.115	4.509	-1.797	39.8	187.6	8.15	4.02	2.18
SB-16	9.25	5.516	25.174	4.498	-1.742	38.7	187.6	7.95	3.92	2.37
SB-17	9.47	5.562	25.104	4.787	-1.916	40.0	187.6	8.65	4.26	2.74
SB-18	9.68	5.529	25.138	4.775	-1.658	34.7	187.6	7.54	3.72	3.28
SB-19	9.87	5.518	25.110	4.777	-1.384	29.0	187.6	6.30	3.11	3.86
SB-20	10.01	5.506	25.768	4.661	-1.164	25.0	187.6	5.45	2.69	4.59
SB-21	10.17	5.509	25.157	4.937	-1.205	24.4	187.6	5.50	2.71	6.18
SB-22	10.32	5.540	25.165	4.926	-1.060	21.5	187.6	4.81	2.37	8.10
SB-23	10.55	5.558	25.156	4.926	-0.800	16.2	187.6	3.62	1.79	12.52

Table 3. Summary of the B adsorption experiments on $SiO_{2(am)}$ conducted in $CaCl_2$ 0.01 M medium.

run #	pH	$SiO_{2(am)}$	Solution	$[B]_0$	$\Delta[B]$	$\%B_{ads}$	SSA	B_{ads}	B_{ads}	[Si]	[Ca]	[Na]
		g	g	ppm	ppm		m^2/g	µg/g	nmol/m^2	mmol/kg	mM	mM
SB-31	6.05	6.065	25.170	4.956	-0.874	17.6	159.3	3.62	2.10	5.09	5.76	4.37
SB-24	6.38	5.492	25.119	4.862	-0.568	11.7	187.9	2.60	1.28	1.61	-	-
SB-25	6.65	5.452	25.146	4.836	-1.427	29.5	187.9	6.58	3.24	1.91	-	-
SB-32	7.00	5.558	25.110	4.962	-1.944	39.2	159.3	8.78	5.10	6.83	2.76	14.88
SB-26	7.23	5.456	25.030	4.857	-1.954	40.2	187.9	8.97	4.41	3.09	-	-
SB-27	7.78	5.453	25.840	4.701	-2.472	52.6	187.9	11.71	5.77	2.45	-	-
SB-33	8.02	5.550	25.130	4.958	-2.796	56.4	159.3	12.66	7.35	6.24	0.46	20.74
SB-28	8.21	5.455	25.105	4.821	-3.001	62.2	187.9	13.81	6.80	2.33	-	-
SB-29	8.56	5.463	25.174	4.810	-3.112	64.7	187.9	14.34	7.06	2.39	-	-
SB-34	8.98	5.566	25.141	4.971	-3.085	62.1	159.3	13.93	8.09	3.79	0.039	21.87
SB-30	9.04	4.710	25.135	4.783	-2.859	59.8	187.9	15.25	7.51	2.35	-	-
SB-35	9.09	5.535	25.103	4.962	-2.946	59.4	159.3	13.36	7.76	4.09	0.030	21.92
SB-36	9.26	5.560	25.177	4.960	-2.899	58.5	159.3	13.13	7.62	3.04	0.020	22.31

Table 4. Boron isotopic data for the adsorption experiments conducted in NaCl and $CaCl_2$ 0.01 M aqueous solutions. The isotopic composition of the starting NaCl and $CaCl_2$ 0.01 M solutions correspond to $\delta^{11}B_0$ = -0.05 ±0.06 ‰ and -0.15 ±0.06 ‰, respectively.

run #	pH	$X_{B\text{-}ads}$	$\delta^{11}B_{sol} \pm 2\sigma$ (‰)	$\delta^{11}B_{ads} \pm 2\sigma$ (‰)	$\Delta^{11}B_{ads\text{-}sol} \pm 2\sigma$ (‰)	$\alpha_{ads\text{-}sol} \pm 2\sigma$
NaCl 0.01 M						
SB-01	6.61	0.107	1.62 ±0.34	-13.96 ±3.36	-15.58 ±3.38	0.985 ±0.003
SB-03	6.97	0.177	2.85 ±0.21	-13.57 ±3.63	-16.42 ±3.63	0.984 ±0.001
SB-02	7.01	0.130	3.03 ±0.13	-20.70 ±6.37	-23.73 ±6.37	0.977 ±0.002
SB-04	7.14	0.168	4.09 ±0.24	-20.59 ±2.04	-24.68 ±2.06	0.976 ±0.002
SB-05	7.62	0.259	6.23 ±0.13	-18.01 ±1.01	-24.24 ±1.02	0.976 ±0.001
SB-06	7.93	0.291	8.51 ±0.13	-20.95 ±1.02	-29.47 ±1.03	0.971 ±0.001
SB-07	7.94	0.272	7.02 ±0.03	-18.95 ±0.94	-25.96 ±0.94	0.974 ±0.001
SB-08	8.06	0.255	7.72 ±0.05	-22.73 ±1.20	-30.45 ±1.21	0.970 ±0.001
SB-09	8.16	0.247	8.36 ±0.14	-25.72 ±1.45	-34.08 ±1.46	0.966 ±0.001
SB-10	8.27	0.300	9.13 ±0.08	-21.53 ±0.99	-30.66 ±0.99	0.970 ±0.001
SB-11	8.42	0.317	9.41 ±0.20	-20.43 ±0.97	-29.85 ±0.99	0.971 ±0.001
SB-12	8.56	0.410	9.39 ±0.19	-13.67 ±0.56	-23.06 ±0.59	0.977 ±0.001
SB-13	8.73	0.408	9.26 ±0.27	-13.56 ±0.63	-22.82 ±0.68	0.977 ±0.001
SB-14	8.9	0.361	8.81 ±0.06	-15.72 ±0.62	-24.53 ±0.63	0.976 ±0.001
SB-15	9.05	0.398	7.78 ±0.09	-11.87 ±0.46	-19.65 ±0.47	0.981 ±0.000
SB-16	9.25	0.387	6.38 ±0.10	-10.23 ±0.42	-16.61 ±0.44	0.984 ±0.000
SB-17	9.47	0.400	4.95 ±0.16	-7.55 ±0.38	-12.50 ±0.41	0.988 ±0.000
SB-18	9.68	0.347	3.27 ±0.06	-6.30 ±0.31	-9.57 ±0.32	0.990 ±0.000
SB-19	9.87	0.290	2.08 ±0.11	-5.27 ±0.41	-7.35 ±0.43	0.993 ±0.000
SB-20	10.01	0.250	1.61 ±0.16	-5.06 ±0.59	-6.67 ±0.61	0.993 ±0.001
SB-21	10.17	0.244	1.01 ±0.12	-3.36 ±0.48	-4.37 ±0.50	0.996 ±0.000
SB-22	10.32	0.215	0.75 ±0.03	-2.97 ±0.33	-3.72 ±0.33	0.996 ±0.000
SB-23	10.55	0.162	0.21 ±0.20	-1.39 ±1.07	-1.59 ±1.09	0.998 ±0.001
$CaCl_2$ 0.01 M						
SB-24	6.38	0.117	5.38 ±0.12	-41.99 ±4.95	-47.37 ±4.95	0.954 ±0.005
SB-25	6.65	0.295	9.60 ±0.10	-23.44 ±1.10	-33.04 ±1.11	0.968 ±0.001
SB-26	7.23	0.402	13.93 ±0.05	-21.05 ±0.75	-34.98 ±0.75	0.966 ±0.001
SB-27	7.78	0.526	17.25 ±0.26	-15.84 ±0.56	-33.09 ±0.62	0.967 ±0.001
SB-28	8.21	0.622	19.20 ±0.34	-11.89 ±0.45	-31.08 ±0.56	0.969 ±0.001
SB-29	8.56	0.647	17.03 ±0.08	-9.52 ±0.34	-26.55 ±0.35	0.974 ±0.000
SB-30	9.04	0.598	12.82 ±0.11	-8.88 ±0.31	-21.70 ±0.33	0.979 ±0.000

Table 5. Surface complexation reactions for B adsorption at the $SiO_{2(am)}$-water interface and B isotope fractionation factors between adsorbed surface species and aqueous solution. The listed values of the intrinsic stability constants refer to the models that best describe the experimental data acquired from NaCl and $CaCl_2$ aqueous solutions. For NaCl solutions, Model #2 provides more consistent results than Model #1 (see text). The corresponding fractionation factors of tetrahedral and trigonal surface species relative to $B(OH)_{3(aq)}^0$ were determined assuming α_{3-4}=1.027. The other corresponding model parameters are listed in Table 1.

Aqueous fluid	**Surface reaction**	$Log\ K_{int}^0$ **(25 °C. *I = 0*)**	**R**	α_{B3-is}	α_{B4-is}	α_{B4-os}
NaCl 0.01 M ***Model #1***	$>SiOH^0 + B(OH)_3^0 = SiOB(OH)_2^0 + H_2O$	-0.44 ± 0.10	0.99	0.9849 ±0.0030	-	-
	$>SiOH^0 + B(OH)_3^0 = SiOB(OH)_3^- + H^+$	-7.84 ± 0.11		-	0.9589 ±0.0024	-
	$>SiOH^0 + B(OH)_3^0 + H_2O = SiOH_2^+ - OB(OH)_3^{2-} + H^+$	-8.74 ± 0.18		-	-	0.9861 ±0.0030
NaCl 0.01 M ***Model #2***	$>SiOH^0 + B(OH)_3^0 = SiOB(OH)_2^0 + H_2O$	**-0.56 ± 0.23**	**0.98**	**0.9841 ±0.0025**	**-**	**-**
	$>SiOH^0 + B(OH)_3^0 = SiOB(OH)_3^- + H^+$	**-7.64 ± 0.06**		**-**	**0.9685 ±0.0020**	**-**
$CaCl_2$ 0.01 M	$>SiOH^0 + B(OH)_3^0 = SiOB(OH)_3^- + H^+$	**-8.36 ± 0.14**	**0.98**	**-**	**0.9671±0.0017**	**-**
	$>SiO^- - Ca^{2+} + B(OH)_4^- => SiO^- - CaB(OH)_4^+$	**1.63 ± 1.12**		**-**	**-**	**-**